UNIVERSITÀ DI SIENA 1240

UNIVERSITA' DI SIENA

DIPARTIMENTO DI MEDICINA MOLECOLARE E DELLO SVILUPPO

DOTTORATO DI RICERCA IN MEDICINA MOLECOLARE

CICLO XXXII°

COORDINATORE: Prof. Vincenzo Sorrentino

Increased expression of sAnk1.5 does not predispose to Type 2 Diabetes in transgenic mice.

BIO/17

DOTTORANDA
Dott.ssa Luisa Raucci

TUTOR
Prof. Vincenzo Sorrentino

CO-TUTOR
Dott. Enrico Pierantozzi

ANNO ACCADEMICO: 2018/2019

INDEX

Abstract

Skeletal muscle represents about 40% of the body mass and is the site where the major part of blood glucose is disposed following insulin stimulation. Due to this critical role, skeletal muscle dysfunctions often result in the development of systemic metabolic diseases. Type 2 Diabetes (T2D) is the most common chronic metabolic disorder, representing nearly 90% of the overall diabetes cases. T2D is characterized by insulin resistance followed by reduced insulin release from pancreatic β-cells, resulting in high glucose concentration in bloodstream and glucose intolerance. T2D is a multifactorial disorder, as its onset has both genetic and environmental origins.

Genome Wide Association Studies have identified hundreds of single nucleotide polymorphisms (SNPs) associated to T2D susceptibility, in the human genome. Interestingly, several of these SNPs were identified in the *ANK1* locus, although these SNPs were found in regions neither coding nor endowed with a regulatory activity. However, two recent independent studies identified a novel SNP in the internal promoter of the *ANK1* gene, which drives the expression of sAnk1.5, a striated muscle-specific small ANK1 isoform. The sAnk1.5 protein is localized on the sarcoplasmic reticulum (SR) membrane, in skeletal muscle fibers, and interacts with Obscurin, a giant protein of the sarcomere. This interaction stabilizes the SR and guarantees the close apposition of this organelle around the contractile apparatus. The ANK1 internal promoter carrying the C/C variant displays higher transcriptional activity with respect to the T/T variant. Accordingly, skeletal muscle biopsies of individuals carrying the C/C genotype showed higher levels of both sAnk1.5 mRNA and protein compared to those carrying the T/T genotype.

The aim of this thesis was to investigate whether sAnk1.5 overexpression in skeletal muscle might predispose to T2D susceptibility. Accordingly, we generated a transgenic mouse model with the coding sequence of the murine sAnk1.5 under the transcriptional control of the skeletal muscle-specific rat myosin light chain promoter. In these transgenic mice, protein levels of sAnk1.5 were increased up to 50% in skeletal muscles with respect to wild

type mice. Basal glucose levels, glucose and insulin tolerance were monitored over a period of 12-months. In addition, 2-months old mice were fed with a high fat diet for twelve weeks. The results obtained did not reveal significant differences in glucose and insulin disposal between transgenic and wild type mice.

In conclusion, our results, show that sAnk1.5 overexpression does not appear to predispose to a pre-diabetic or diabetic condition.

Introduction

1.1 Overview of skeletal muscle

Skeletal muscle comprises approximately 40% of total body weight and represents one of the most dynamic and plastic tissue. It converts the chemical energy to mechanical force guaranteeing voluntary movements, the maintenance of the posture and the functional independence of the body. In addition, it fulfills a non-secondary metabolic role contributing to overall body energy metabolism, to the storage of amino acids and carbohydrates and to the maintenance of the body temperature[1]. Skeletal muscle architecture is characterized by a well-defined mutual arrangement of muscle cells (muscle fibers) organized in bundles, and connective tissue. Muscle fibers are cylindrical structural syncytia, where several nuclei are localized in peripheral regions. Skeletal muscle fibers are characterized by a diameter of 10-100 μm, and display a length that, in humans, may range from 1mm to several centimeters. Each single muscle fiber is enveloped and separated from its neighbors by a connective sheet, the endomysium, which in turn is in continuity with the perimysium, a thicker sheet of connective tissue that surrounds bundles of fibers. The entire muscle is further surrounded by the epimysium, which anchors it to the tendons. These connective layers provide to the maintenance of the overall muscular structure and represent the site where blood vessels and nerves spread into muscle, guaranteeing the nutriments and electrical stimulations to every single fiber[2]. The cytoplasm of the fibers, also called sarcoplasm, in addition to nuclei and "standard" organelles such as mitochondria, Golgi apparatus, lipid droplets, glycogen stores, is characterized by the presence of three evolutionary conserved structures: the myofibrils, which represent the contractile apparatus, the sarcoplasmic reticulum, which is the site where the calcium ions required for contraction are stored, and the T-tubules, which are invaginations of the plasma membrane (sarcolemma) that

participate in forming the triads. Triads are skeletal muscle specific structures, which represent the cytological core of the excitation-contraction coupling.

1.2 Contraction of skeletal muscle fibers

1.2.1 Myofibrils and sarcomere

The largest part of the cytoplasm of skeletal muscle fibers is occupied by myofibrils. Myofibrils are long filaments parallel to each other and to the fiber's longest axis, and their length may reach several centimeters. Myofibrils are made up by two types of contractile myofilaments, named thick and thin filaments. Thick filaments are composed by myosin, while thin filaments are composed by actin. The myosin protein has a hexameric structure made up by two heavy chains at the C-terminal region, and four light chains forming the globular heads of the molecule, in the N-terminal region. Each globular head contains an ATPase domain able to hydrolyze ATP to ADP+Pi, a process required to generate the energy needed for the contraction and relaxation[3]. The actin protein, in turn, is composed by two twisted proto-filaments of filamentous actin (F-actin), each of which is composed by 400 molecules of globular actin (G-actin), thus resembling a row of pearls. Actin myofilaments are bound for their entire length by tropomyosin proteins, associated head-to-tail, and by troponin (Tn) complexes regularly-spaced by 40nm on tropomyosin. Troponin is a protein complex formed by three subunits: troponin C (TnC), troponin I (TnI) and troponin T (TnT). When Ca^{2+} is released from the lumen of sarcoplasmic reticulum (SR), it binds to TnC, inducing a conformational change that results in TnT release from the inhibitory action of TnI. "Activated" TnT allows tropomyosin sliding along the actin filament, which in turn exposes myosin-binding domains on actin filaments, enabling the mechanical interaction between myosin and actin[4,5]. The sliding of thin filaments along thick filaments allows muscle contraction[6]. For decades skeletal muscle fibers were distinguished on the basis of their color as red or white, and on their contractile properties as fast and slow. In addition, fast-twitch muscles, rich in white fibers, where known to have a glycolytic

metabolism and to easily fatigue, while slow-twitch muscles, rich in red fibers, had a high content of myoglobin, mitochondria and were more adapt to sustain a continuous activity. Use of histochemical staining, based on the activity of the myosin ATPase, identified three fiber types: type I present in slow-twitch muscles and type IIa and type IIb, present in fast-twitch muscles. These histochemical differences reflect the type of myosin heavy chain isoforms expressed in these fibers. The type I fibers are slow twitch fibers, rich in mitochondria, with an oxidative metabolism and are fatigue resistant. Type IIa are fast twitch fibers with glycolytic but also oxidative metabolism, which makes them partly fatigue resistant, although less than type I fibers. Type IIb are glycolytic fast-twitch fibers with a lower number of mitochondria, are involved in short-lasting and powerful contractions but are more susceptible to fatigue. An additional type of fibers, IIx, expressing another myosin heavy chain isoform, MHCIIx are characterized by an intermediate metabolic and twitch properties intermediate to those of type IIa and IIb fibers[7,8,9]. The distribution of these different fibers depends on muscle actions.

Contractile myofilaments are arranged to form the smallest contractile unit of skeletal muscle fibers: the sarcomere. The reciprocal disposition of myosin and actin generates regularly-spaced regions that differentially reflect polarized light, forming a highly ordered sequence of anisotropic and isotropic bands, when observed under the microscope. The presence of these alternate bands is the reason why the skeletal muscle fibers are defined “striated”. Anisotropic (dark) and isotropic (light) bands are known as A band and I band, respectively. In the center of each A band is present a lighter zone, called H band, crossed in the middle by a transversal structure, the M band. The I band is crossed in the middle by a darker line, the Z disk. Each sarcomere is composed by an entire A band flanked by two moieties of an I band. As a consequence, every single sarcomere extends between two Z disks, with the M band in the middle (Fig. 1). The lateral and longitudinal regular alignment of hundreds of sarcomeres with respect to the longest axis of the muscle fibers form the myofibrils[2].

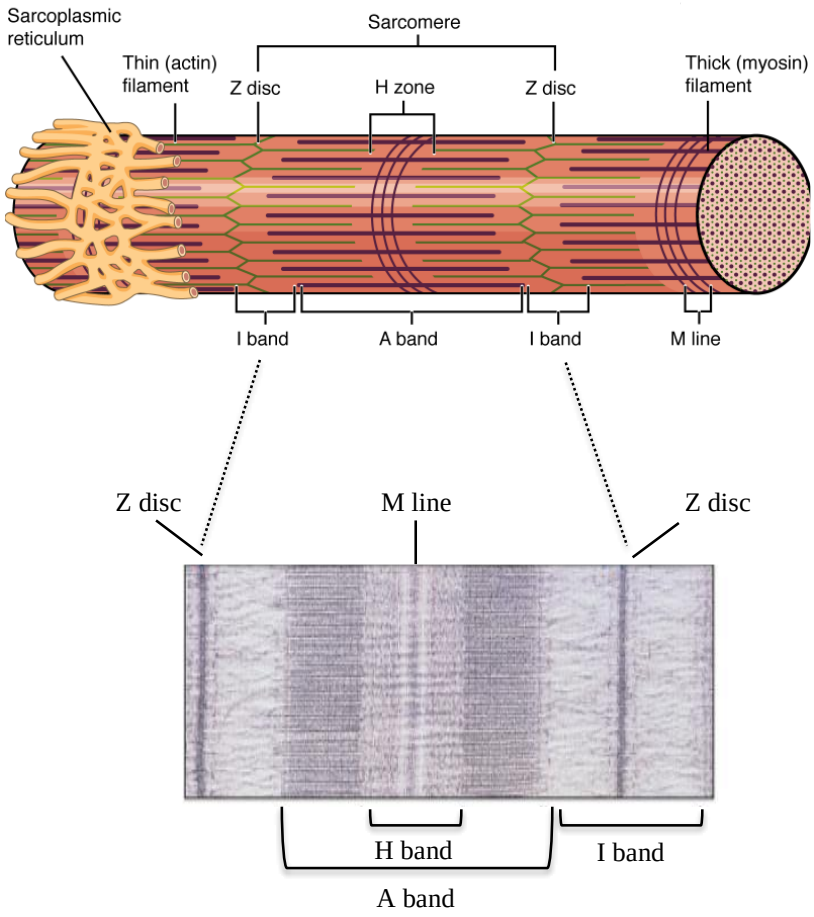

Figure 1: Structure of the sarcomere. In the upper cartoon, reciprocal actin and myosin filaments disposition in the sarcomere, which give rise to striation (Bands A and I, and H-zone are indicated), is depicted. Z- disks and M-bands of two adjacent sarcomeres are indicated. In the lower picture, an image acquired with the electron microscope of a sarcomere is reported. The image was adapted from Luther, 2009[10].

Three additional giant proteins, namely titin, obscurin and nebulin[1], participate in the proper organization of the sarcomeric scaffold, also contributing to mechanical and physiological properties of muscle fibers (Fig. 2). Titin (~3800 kDa) is anchored on both M band and Z disk with its N-terminal and C-terminal regions, respectively. On the M-band, titin interacts with obscurin and myomesin, contributing to M-band stability, while it binds to obscurin and α-actinin on Z disk[11]. As a consequence, two molecules of titin generate a protein backbone that spans along the entire sarcomere length. Nebulin (800 kDa) anchors at the Z-disk and elapses for the entire length of the actin filaments, thus providing mechanical support for thin filaments positioning, length, and spacing[12]. Obscurin (850 kDa) is a sarcomeric protein mainly present at the M-

band and at a lesser extent at Z-disk. Initially identified as a titin-interacting protein[13,14], it has been later reported that Obscurin interacts with a muscle-specific protein localized in the SR, namely small ankyrin 1.5 (sAnk1.5); this association is responsible for the proper positioning of the SR around myofibrils [15,16,17]. Recent studies on Obscurin knockout mice also indicated that obscurin is required for the overall M-band stability[18,19]. In addition, obscurin is involved in ankyrinB-dependent dystrophin localization and overall sarcolemma integrity[19]. Dystrophin (427 kDa) is localized in correspondence of the Z-disk and is part of a protein complex called Dystrophin Glycoprotein Complex (DGC). This structure is the core of costamere, a multi-protein complex of the sarcolemma localized in correspondence of the Z-disks. This complex acts as a bridge between fiber actin cytoskeleton and the extracellular matrix, in order to dissipate the mechanical stress generated by repeated cycles of contraction and to protect the integrity of the sarcolemma[20].

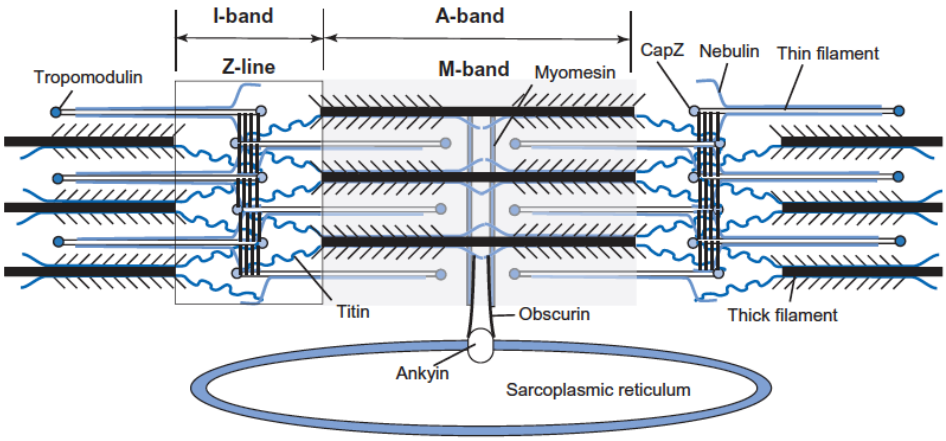

Figure 2: Localization of sarcomere scaffold protein titin, nebulin and obscurin. Titin is anchored on both M band and Z disk; as a consequence, two molecules of titin generate a protein backbone that spans along the entire sarcomere length. Nebulin is anchored on the Z-disk and elapses for the entire length of the actin filaments, thus providing mechanical support for thin filaments positioning, length, and spacing. Obscurin is present at the M-band and at a lesser extent at Z-disk; in correspondence of M-band interacts with sAnk1.5 positioning correctly the SR around myofibrils. The image was taken from Feher, 2017 [21].

1.2.2 Sarcoplasmic reticulum, T-tubule, triad and excitation-contraction coupling

The SR is a specialized form of endoplasmic reticulum where calcium ions (Ca^{2+}) are stored. The SR regulates both Ca^{2+} release following motor neurons stimulation, allowing muscle contraction, and Ca^{2+} reuptake from the cytosol to the SR lumen, leading to muscle relaxation[22,23]. The SR is composed by two different compartments: the longitudinal SR (l-SR) and the junctional SR (j-SR or terminal cisternae). l-SR is formed by anastomosed tubular structures generating a network that wraps myofibrils in correspondence of both A- and I-bands of sarcomeres (Fig.3).

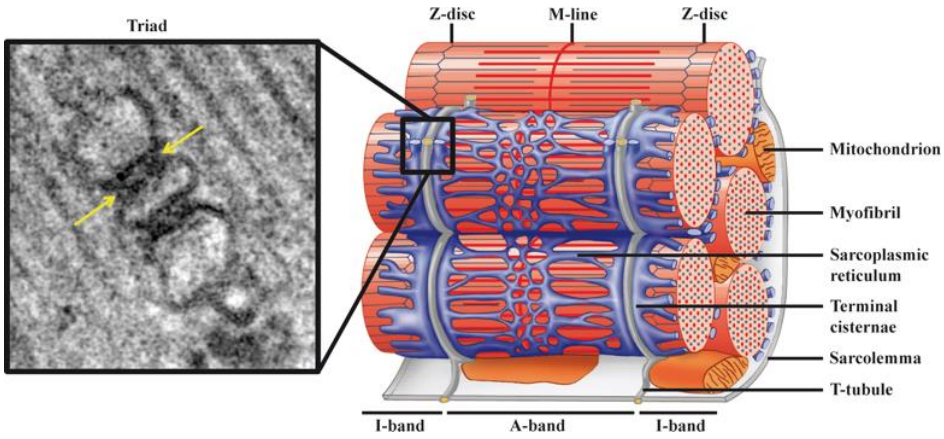

Figure 3: Triad organization in skeletal muscle. The right panel is a schematic representation of the triad: one T-tubule, a sarcolemma invagination, is flanked by two terminal cisternae, generating the triad, the intracellular structure where the E-C coupling occurs. The triads localize in correspondence of every A-I bands border. The left panel is an image of triad junction acquired with electron microscopy, where the arrows indicate the T-tubule flanked by the terminal cisternae. The image was taken from Al-Qusairi et al, 2011 [24].

At their distal ends, l-SR tubules coalesce into dilated structures called terminal cisternae, which form the j-SR, localized at the border between A-band and I-band. In correspondence of every A-I bands border, two terminal cisternae flank the T-tubule, an invagination of the sarcolemma into the sarcoplasm. The structure composed by a T-tubule and the two terminal cisternae is called triad. Triads are the structures where the electrical signal initiated by motor neurons stimulation is converted into the chemical signal represented by calcium

release from the SR. This process allows the excitation-contraction (E-C) coupling mechanism, essential for proper muscle contraction (Fig. 4).

The E-C coupling starts with the release of acetylcholine by the motor neuron, that binds its specific receptors on the sarcolemma inducing the membrane depolarization. When depolarizing wave reaches the T-tubule, it determines the conformational change of dihydropyridine receptor (DHPR), a voltage gated calcium channel specifically localized on the T-tubule membrane. The conformational change of DHPR allows its physical interaction with the ryanodine receptors, RyRs, calcium channels located on the membrane of the j-SR. In mammals, three RyR isoforms, encoded by three different genes, have been identified: RyR1, RyR2, and RyR3[20]. In skeletal muscle, RyR1 is the main expressed isoform. RyR1, once bound by DHPR, changes its conformation allowing massive Ca^{2+} release from terminal cisternae into fiber cytoplasm. Raising of Ca^{2+} ions cytoplasmic concentration, $[Ca^{2+}]_{cyt}$, in the fibers results in tropomyosin sliding along thin filaments, representing the initial event for proper actin-myosin interaction[25].

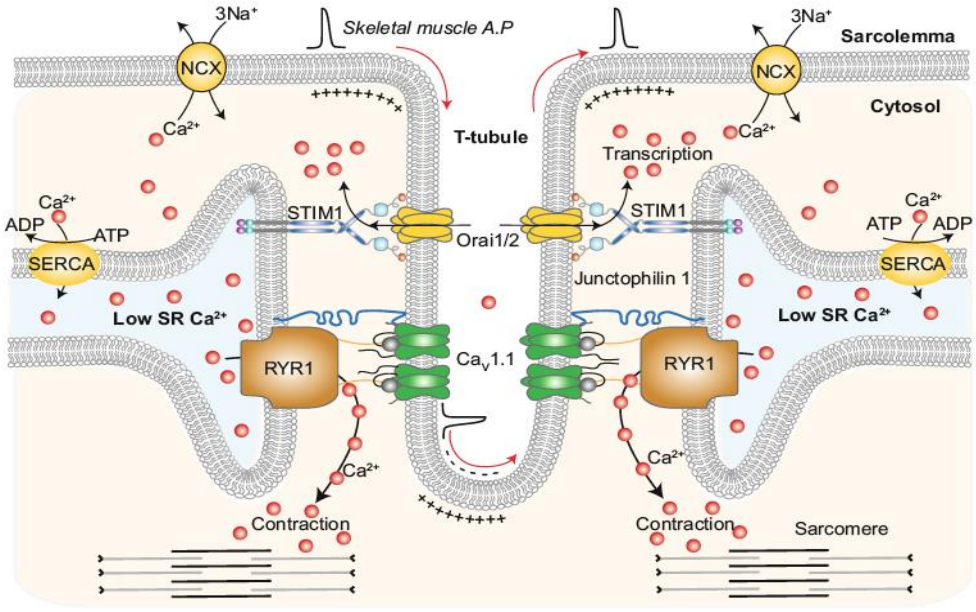

Figure 4: Excitation-contraction mechanism. The T-tubule, a sarcolemma invagination, is flanked by two terminal cisternae, generating the triad, the intracellular structure where the electrical signal initiated by motor neurons stimulation is converted into the chemical signal represented by calcium release from the SR. When the nervous stimulus occurs, the depolarization wave spread all along the T-tubule, resulting in a conformational change in DHPR, the voltage gated calcium channel present on its membrane. This conformational change allows the physical interaction of DHPR with RyR1, a calcium channel present on the terminal cisternae membranes. This interaction leads RyR1 activation with the release of calcium ions from the SR lumen to the cytosol. The increased concentration of calcium allows the sliding between thick and thin myofilaments. The image was taken from Dickson, 2017[26].

Tropomyosin sliding enables the formation of the actin-myosin complex. The ATPase domains of myosin heads hydrolyze ATP, producing the energy required for myosin movement and sarcomere shortening. Myosin flexes of nearly 45° pulling the actin filament of about 10 nm in the direction of the M band. As a consequence, during contraction sarcomeres shorten, and the width of the I-bands is reduced due to the sliding of thin filaments on thick filaments (Fig.5). To ensure an immediate subsequent new contraction cycle ADP unbinds, and a new ATP molecule binds to myosin heads, thus unfastening myosin from the actin filaments. The hydrolysis of new ATP in ADP+Pi initiates a new cycle of contraction.

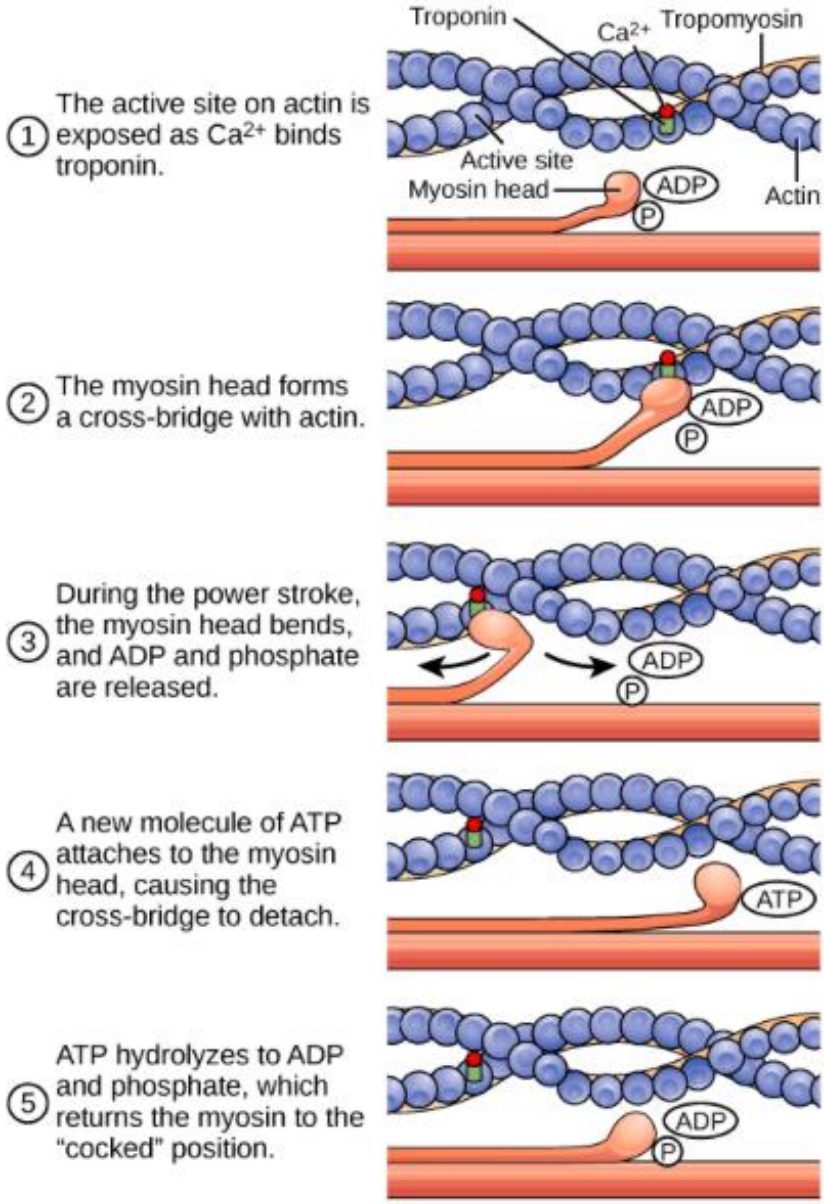

Figure 5: Model of cyclic sliding of thin filaments during the contraction. ATP is hydrolyzed by the ATPase domains of myosin heads, producing the energy required the attachment of myosin to actin filaments. When the Pi produced by ATP hydrolysis is released, myosin heads flexes of nearly 45° pulling thin filaments in direction of the M-band and the sarcomere shortening.

In order to allow muscle relaxation at the end of the contraction, resting $[Ca^{2+}]_{cyt}$ must be restored. This function is provided by the action of Ca^{2+} pumps that use energy produced by the hydrolysis of ATP to actively pump Ca^{2+} from the cytoplasm into the SR lumen. These pumps are represented by Sarco/Endoplasmatic Reticulum Ca^{2+} ATPase (SERCA) pumps, which are

localized on the membrane of the l-SR. For every single hydrolyzed ATP, SERCA pumps transport two calcium ions inside the SR.

Muscle contraction and SERCA pumps activity are processes that require high-energy expenditure, which is mainly satisfied by the hydrolysis of ATP. However, muscle fibers have limited ATP deposits, which would allow only short-lasting maximum efforts; therefore, in order to ensure the energy required for prolonged muscle contraction, it is of paramount importance that ATP is continuously regenerated.

1.3 Energetic metabolism

The energetic metabolism comprises all the reactions required to produce free energy to fulfill biosynthesis processes, to maintain body temperature, and to support any type of work that cells must accomplish. Catabolic reactions release energy, while the anabolic reaction require energy. The intermediate molecule between the catabolic and anabolic reactions is the adenosine-triphosphate (ATP) molecule, whose hydrolysis in ADP+Pi is used by all types of cells to obtain free energy for all their activities. To regenerate ATP, ADP is continuously reconverted in ATP by the mitochondria. Free energy necessary for this latter process is obtained by the oxidation of carbohydrates, proteins and fatty acids. Indeed, cells can obtain around 40% of required free energy from glucose oxidation. Glucose oxidation takes place through three consequential metabolic processes: glycolysis, Krebs cycle and oxidative phosphorylation[27].

Glycolysis is the first step of glucose oxidation. It does not require oxygen and occurs in cell cytoplasm. This process is not sufficient to sustain the energy requirement of the cells, because the partial oxidation of glucose in two pyruvate molecules yields only two molecules of ATP and two molecules of NADH. To obtain additional ATP and reducing molecules, pyruvate acids are transported into the mitochondria where they enter the Krebs cycle, at the end of which, they are completely oxidized in CO_2 and H_2O, with the simultaneous release of 2 ATP, 8 NADH and 2 $FADH_2$. The last step of glucose oxidation is the oxidative phosphorylation, in which NADH and $FADH_2$ are further

oxidized to release H^+ and free electrons. The electrons are transferred to enzymes able to pump the H^+ ions outside the mitochondria, generating an inward protonic gradient. The energy provided by this proton motive force is used by the ATP synthase to convert ADP in ATP. As a result of all these processes, the oxidation of a single glucose molecule yields 36 ATP molecules[2]. Indeed, glucose is the main source of free energy for the cells.

1.3.1 Role of skeletal muscle in metabolism

During exercise, skeletal muscle requires an energy expenditure which increases by about 20-30 folds. As a consequence, during prolonged contraction, skeletal muscles deplete an amount of ATP which is about 1000-fold higher compared to resting conditions[28]. It is important to note that both muscle contraction and relaxation are involved in energy consumption. Indeed, during contraction, myosin proteins hydrolyze ATP to allow the sliding of thin filaments, while during relaxation, SERCA pumps, hydrolyze ATP molecules to reuptake Ca^{2+} ions from cytosol to the SR lumen[29]. In addition, skeletal muscle tissue, being involved in the regulation of body temperature, also consumes ATP following shivering, which is a mechanism that allows regulation of thermogenesis by generating heat through repetitive muscle contractions[29].

Based on these different ATP-consuming mechanisms, skeletal muscle tissue plays an important role in regulating absorption and systemic homeostasis of glucose.

Glucose is a monosaccharide obtained by the hydrolysis of carbohydrates (disaccharides and polysaccharides) taken from the diet. Molecules of glucose are absorbed by the intestine and then transferred to the bloodstream, from which it is either uptake by all tissues or it can be stored in both liver and skeletal muscles as glycogen. During fasting condition, glucose is released in the bloodstream following the activation of specific mechanisms such as glycogenolysis or gluconeogenesis. Blood glucose concentration varies during the day: in fasting condition glycaemia levels are around 60-90mg/dl of blood, while glucose levels became higher (140mg/dl) following food intake.

Glucose is a hydrophilic molecule that cannot freely penetrate the lipid bilayer of the membranes. Thus, specific glucose transporters are required (Fig 6).

Glucose transport from the extracellular to the intracellular compartments occurs through both an active transport and an ATP-independent facilitated diffusion mechanism. The active transport is present in the intestine and renal tubules, where SGLUT carriers allow glucose uptake against its concentration gradient using the biochemical energy obtained by a Na^{+}/glucose co-transport[30]. In contrast, in the vast majority of tissues, ATP-independent facilitated diffusion mechanism occurs along glucose concentration gradient through the GLUT transporters family, and do not require energy consumption[31]. GLUT proteins are a family of glucose transporters composed of twelve membrane spanning helices and a large intracellular loop that connect the sixth and the seventh helices[32].

All transporters isoforms share a homology in their sequence, with a domain rich in tryptophan and glycine residues, necessary to glucose translocation across the plasma membrane. GLUT transporters have been classified into three classes based on sequence similarities, pattern of tissue expression, transport kinetics and regulated expression in different physiological conditions.

Class I comprises:

- GLUT1 transporters, which are expressed in the nervous cells and erythrocytes;
- GLUT2 transporters, which are expressed in the liver, kidneys and β-cells of pancreas;
- GLUT3 transporters, with a high affinity for the glucose, which are expressed in tissue that need high amount of energy such as nervous tissue;
- GLUT4 transporters, which are expressed in adipose tissue and striated muscles, and are the only insulin-responsive glucose transporters.

Class II comprises:

- GLUT5 transporters, which are expressed in testis and in small intestine;
- GLUT7 transporters, which are expressed in the intestine;

- GLUT 9 transporters, which are expressed in the liver and kidneys.

Class III comprises GLUT6-8-10-12-13 transporters in which the glycosylation site is located on loop 9, at variance of transporters belonging to Class I and II, in which the glycosylation site resides on loop1[33,34,35]

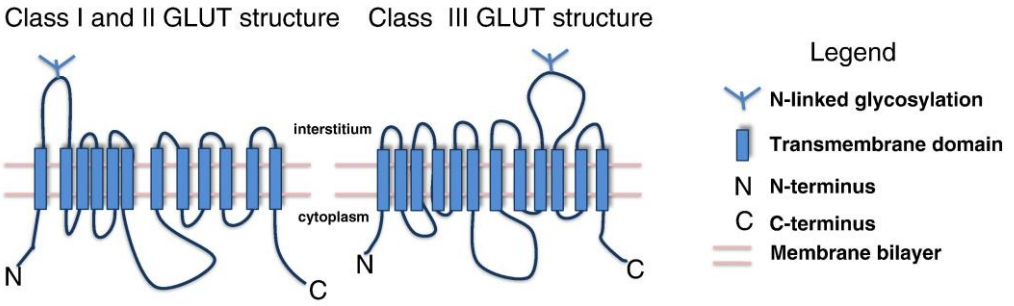

Figure 6: Structure of GLUT transporters. All isoforms of glucose transporters are composed of twelve membrane spanning helices and a large intracellular loop that connect the sixth and the seventh helices; the N- and C-terminal regions of the glucose transporters reside in the cytoplasmic space. The glycosylation site resides in the extracellular space and is located on loop 1 and loop 9 of GLUT belonging to Class I-II and Class III, respectively. The image was taken from Barron et al, 2016[36].

GLUT4 is the main glucose transporter expressed in skeletal muscle, heart and adipose tissue. Following translation, GLUT4 is stored in intracellular vesicles, known as GLUT4 storage vesicles (GSVs), localized in proximity to the plasma membrane. GSVs reside in the intracellular compartment until the activation of specific molecular pathways promote their translocation and fusion with the plasma membrane, allowing the exposition of GLUT4 transporters on the extracellular side[32]. The main stimuli that regulate GLUT4 vesicles trafficking are insulin and muscle contraction[37]. Both pathways increase glucose uptake by about 10 to 20-folds[38]. In fact, in basal condition, 5-10% of GLUT4 transporters present in a given cell are exposed on the membrane. This percentage became higher (20-50%) as a consequence of its mobilization.

1.3.2 Insulin-dependent GLUT4 translocation

The high amount of glucose in bloodstream in the post prandial period leads to insulin release from the β cells of pancreas. Insulin is a peptide hormone (6kDa), composed by two chains connected to each other through disulfide bonds. This hormone interacts with its receptor, present on the target tissues. The insulin receptor (IR) is a tyrosine-kinase receptor, composed by two α subunits, on the extracellular side, and two transmembrane β subunits. The interaction between the insulin and its receptor generates a conformational change of α subunits, allowing the auto-phosphorylation of tyrosine residues present on β subunits. These phosphorylated residues allow the recruitment of insulin receptor substrates, such as IRS1, IRS2, IRS3, IRS4 that, through conformational changes, phosphorylate themselves and activate intracellular signaling transduction cascades[37]. Phosphorylated IRSs recruit phosphatidylinositol 3-kinase (PI3K) and activate its catalytic subunit p110, leading to the generation of phosphatidylinositol 3 phosphate (PIP3). PIP3 accumulates on the intracellular side of the sarcolemma and, through additional signaling molecules, activate the phosphoinositide-dependent kinase-1 (PDK1) resulting in the phosphorylation and activation of AKT[39].

AKT is a protein kinase that activates the GTPase activity of AS160 protein. AS160 inhibits RAB10, a G-protein involved in the vesicular trafficking. In the absence of insulin stimulation, RAB10 is in its GDP-bound inactive form, maintaining the intracellular compartmentalization of GLUT4. When the insulin stimulus occurs, the inactivation of AS160 by phosphorylated AKT leads to the generation of the GTP-bound active form of RAB10 protein that in turn allows the translocation of GLUT4 vesicles[40] (Fig.7).

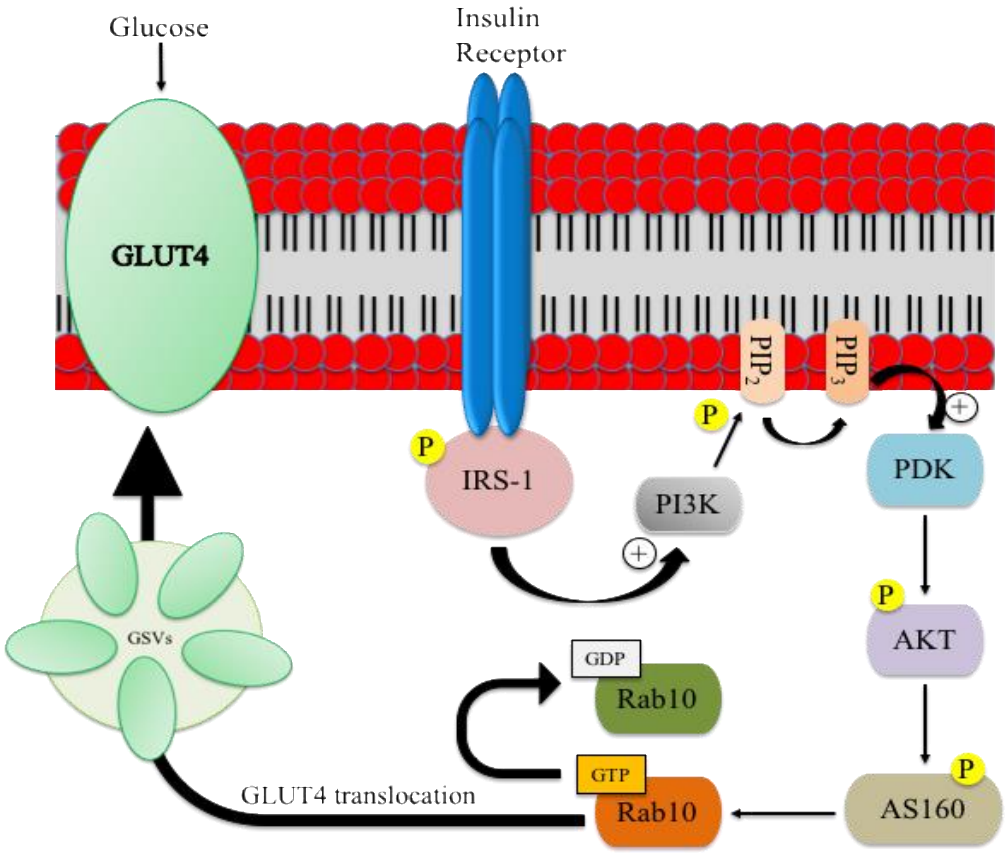

Figure 7: Insulin-dependent pathway for GLUT4 vesicles translocation. The insulin receptor is a tyrosine kinase receptor, which dimerizes and auto phosphorylates following the binding of insulin. The activated receptor triggers and phosphorylates the insulin receptor substrate 1 (IRS-1) on tyrosine residues, which then recruits PI3K and activates its catalytic subunit p110. PI3K catalyzes the phosphorylation of phosphatidylinositol bisphosphate (PIP2) at the plasma membrane to PIP3, which then activates PIP3-dependent kinase (PDK) and then AKT. Through its target, AS160, AKT regulates the activity of Rab10, a G protein involved in the vesicular trafficking. The image was adapted from Thorn et al, 2013[41].

1.3.3 Insulin-independent GLUT4 translocation

Insulin pathway is not the only molecular mechanism that regulates GLUT4 translocation. Indeed, muscle contraction is able to promote GLUT4 vesicular trafficking. In fact, muscle contraction, by consuming ATP, requires high amount of glucose.

ATP hydrolysis increases sarcoplasmic concentration of adenosine monophosphate (AMP), activating the AMP-dependent kinase (AMPK). AMPK is a heterotrimeric complex composed by an α catalytic subunit and β

and γ regulatory subunits, which are both important for target specificity and for complex stability. The interaction between AMP and AMPK leads to the phosphorylation of tyrosine residues present in the kinase domain of the α subunit[42], resulting in the activation of the kinase. Activated AMPK phosphorylates AS160 (also known as TBC1D4) and TBC1D1, two RAB GTPase activating proteins, allowing the translocation of GLUT4 vesicles toward the plasma membrane[43].

Additional insulin-independent mechanisms of GLUT4 translocation involve calcium, bradykinin, nitric oxide and reactive oxygen species by activating molecular mechanisms that partially overlap with insulin- and AMPK-dependent pathways (Fig.8). Increased Ca^{2+} concentration during muscle contraction activate both protein-kinase C (PKC) and Ca^{2+}/calmodulin-dependent protein kinase II (CAMKII). These kinases are able to phosphorylate AMPK, activating the AMPK-dependent GSVs translocation. The hormone bradykinin, beyond regulating physiological events such as inflammation and vascular permeability, is also involved in glucose metabolism. Bradykinin enhances IRS1 tyrosine phosphorylation, promoting its interaction with p85α, the PI3K regulatory subunit[44]. Nitric oxide and reactive oxygen species, produced by mitochondrial activity, promote glucose uptake, although the molecular mechanisms underlying this intracellular signaling have not been fully elucidated yet[45].

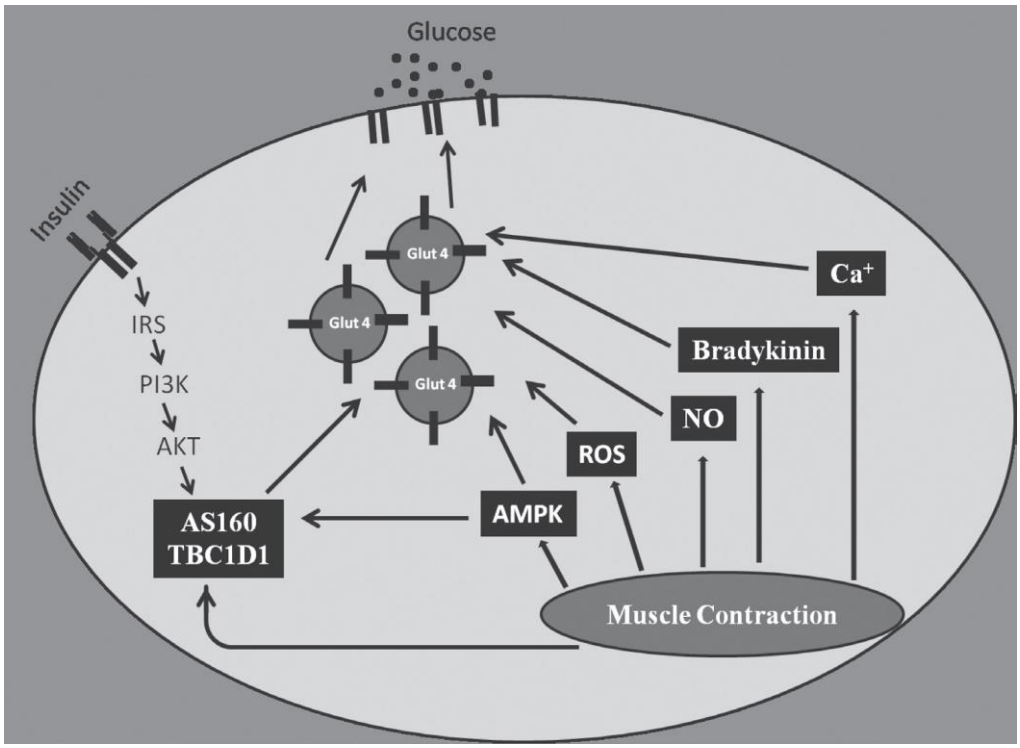

Figure 8: Insulin-independent pathway for GLUT4 vesicles translocation. Calcium, bradykinin, nitric oxide and reactive oxygen species by activating molecular mechanisms those partially overlap with insulin- and AMPK-dependent pathways. The image was taken from Alvim et al, 2014[37].

1.3.4 GLUT4 trafficking

When blood glucose concentration increases, skeletal muscle and adipose tissue absorb circulating glucose through the translocation of GSVs from the intracellular storage pools to the plasma membrane.

Following GSVs translocation toward the plasma membrane, exposure of GLUT4 requires GSVs tethering/docking and fusion with plasma membrane.

Insulin stimulus activates small GTPases promoting the cleavage of protein TUG (tether containing a ubiquitin regulatory X domain of GLUT4), which is located at the cis side of Golgi, tethering GSVs to Golgi matrix proteins. Once TUG has been cleaved, GSVs travel along the microtubular network from the perinuclear region to the membrane[38,46], and dock to the plasma membrane through the exocyst complex. Finally GSVs fuse with plasma membrane through SNARE complexes formed by the interaction between v-SNARE on

vesicle membrane and two t-SNAREs, such as Syntaxin and Synaptobrevin, on plasma membrane[47].

GLUT4 transporters are recycled by internalization processes, involving both clathrin-mediated and clathrin-independent endocytosis. In the former pathway, C- and N-terminal domains of GLUT4 are recognized by AP-2, an adapter protein that simultaneously interacts with GLUT4, phospholipids and clathrin. Clathrin forms a triskelion composed by three clathrin heavy chains (190kDa each) and three clathrin light chains (25kDa each) that allow membrane invagination and the formation of clathrin-coated endocytic vesicles. The clathrin-independent endocytosis is linked to the formation of endosomes from regions of the membrane rich in cholesterol. These structures, called caveolae, are membrane invagination stabilized by membrane proteins called caveolins, which interact with cholesterol and sphingolipids that, in turn, form the coating of the endocytic vesicles[48] (Fig. 9). When endocytic vesicles fuse with the endosomal compartment, GLUT4 transporter can be distributed to either plasma membrane or to trans-Golgi network compartment to be inserted in new GSVs. When endocytic vesicles fuse with lysosomes, GLUT4 transporters are definitively broken down [49].

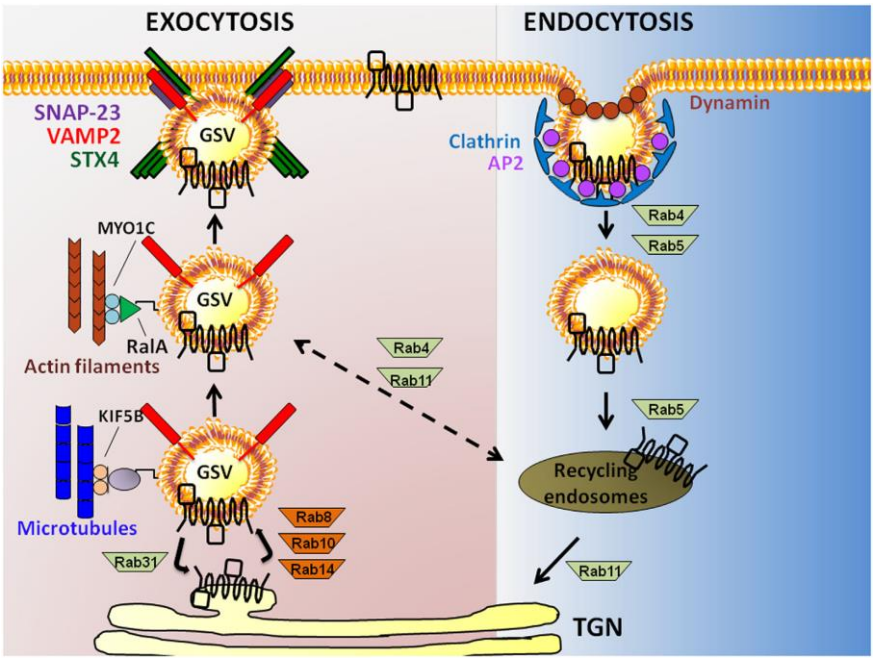

Figure 9: GLUT4 vesicles trafficking. This schematic model shows actin filament and microtubule-dependent exocytosis of GLUT4, and the clathrin-mediated GLUT4 endocytosis. The image was taken from Tunduguru et al., 2017 [38].

1.4 Type 2 Diabetes

Skeletal muscle is the largest insulin sensitive tissue, thus representing the tissue where the major part of glucose (80%) is disposed under insulin stimulation[50]. In addition, glucose uptake by skeletal muscle is also triggered by the insulin-independent pathway activated during exercise, further underlying the importance of skeletal muscle tissue in the regulation of systemic glucose homeostasis[51].

Indeed, skeletal muscle dysfunctions often affect body metabolism, leading to the onset of metabolic disorders[52]. Type 2 Diabetes (T2D) is the most common chronic metabolic disease. This pathology represents the 90% of diabetes cases and is characterized by insulin resistance followed by insufficient insulin release from pancreatic β-cells, resulting in high levels of blood glucose. T2D is a multifactorial disease where environmental (age, lifestyle, obesity, etc.) and hereditary (genetic predisposition) cues are involved in its onset. Although environmental factors play a not-negligible role in the onset of this pathology, they do not impact everyone in the same way. In fact, individuals exposed to similar environmental risks, often display different T2D susceptibility, indicating that genetic factors may account for a higher risk of developing this pathology[53]. In the last decade, the advent of genome wide association studies (GWAS) have permitted to identify hundreds of genetic loci that can be associated to T2D susceptibility, considerably improving the knowledge of those inherited factors that may be causative for the onset of T2D.

1.4.1 *ANK1* locus and Type 2 Diabetes susceptibility

GWAS is an observational study of genetic variants in individuals used to associate genetic variations to particular traits, such as those specific for a given disease. Through GWAS, hundreds of single nucleotide polymorphisms (SNPs) were associated to T2D. The majority of them resides in non-coding sequences, suggesting that the high risk to develop the disease is linked to the genetic regulatory components[54]. In fact, the majority of T2D associated SNPs have been found either in super enhancer sequences and clusters of

transcriptional enhancers, both well known to be involved in cell type specific gene expression[55].

Of note, in the last decade, *ANK1* gene was identified as a locus where several different SNPs associated to T2D susceptibility reside[54]. *ANK1* gene encodes for Ankyrin1, a member of the ankyrin superfamily, first identified in erythrocytes, whose role is to connect the integral membrane proteins with the cytoskeleton.

Soranzo and collaborators[56] identified two variants, rs4737009 and rs6474359, in *ANK1* locus, associated to the production of not-physiological amount of glycated hemoglobin (HbA_{1c}). This modified form of hemoglobin is the result of the glycation reaction, a chemical modification of hemoglobin due to high blood glucose levels. HbA_{1c} is considered a marker for T2D, and these SNPs in *ANK1* gene are currently considered as associated to this metabolic disorder[56]. More interestingly, earlier studies identified, in the *ANK1* locus, the presence of additional SNPs (rs515071 and rs516946), associated to impaired insulin secretion and to defects in β-cells activity[57,58].

1.4.2 Type 2 Diabetes and sAnk1.5

The polymorphisms identified in *ANK1* locus associated to T2D susceptibility are mainly localized in the intron regions of the gene or in those regions without a known regulatory activity. Scott and collaborators, by analyzing 271 skeletal muscle biopsies, revealed the presence, in the regulatory architecture of skeletal muscle, a high number of muscle stretch/super enhancer where specific variants correlate with T2D susceptibility[54]. In particular, two independent GWAS studies identified a SNP (rs508419) associated to T2D susceptibility in the sequence of an internal promoter of the *ANK1* gene (Fig.10). This internal promoter drives the transcription of alternative muscle specific small isoforms of Ankyrin1 (i.e. sAnk1.5, 1.6, 1.7, 1.8, 1.9), among which, sAnk1.5 is by far the most abundant[16,59,60,61].

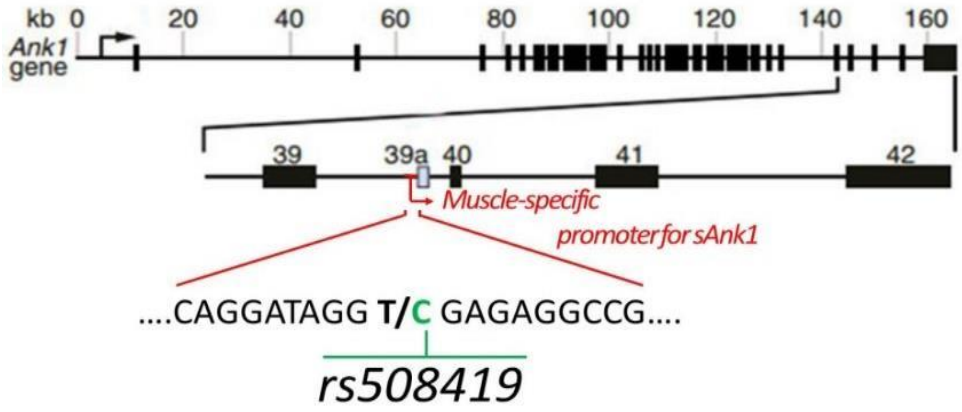

Figure 10: Internal promoter of ANK1 gene, located in the exon 39a, drives only the expression of muscle specific small ankyrin isoforms. The SNP rs508419 resides in the sequence of this internal promoter. The allelic variation associated to T2D susceptibility is underlined in green. The image was adapted by Gallagher, Forget 1998[61].

The rs508419 SNP consists in the substitution of a thymine with a cytosine (C>T) that alters the binding of transcriptional regulators, suggesting a potential increase of promoter activity in subjects carrying C/C allele with respect to those carrying the T/T variant[62,54]. Indeed, *in vitro* luciferase assay performed on C2C12 muscle cells transfected with plasmid carrying C- or T-variants, demonstrated the actual increase of transcriptional activity of the promoter carrying the C-variant. Accordingly, mRNA and protein levels of sAnk1.5 are increased in skeletal muscle of individuals carrying the C/C variant with respect to those carrying the T/T variant (Fig.11).

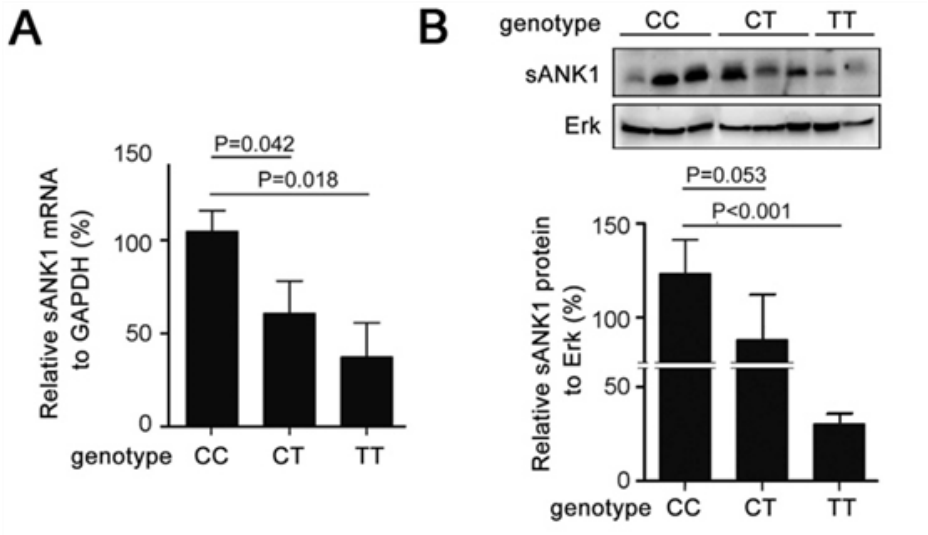

Figure 11: The presence of SNP rs508419 lead to an internal promoter increased activity, resulting in high levels of sAnk1.5 mRNA (A) and protein levels (B) in subjects with C/C allele variant, respect with T/T allele variant. The image was taken from Yan et al., 2016[62].

To initially investigate whether sAnk1.5 increased levels would associate with T2D phenotype, glucose uptake was analyzed in C2C12 muscle cells transfected with sAnk1.5, both in basal condition and insulin-stimulated state. Results obtained from those experiments indicated that glucose uptake was significantly reduced in cells overexpressing sAnk1.5[62].

1.5 Skeletal muscle-specific isoform of Ank1: sAnk1.5

Although the potential involvement of sAnk1.5 in T2D susceptibility has been very recently suggested, to date, the structural role of sAnk1.5 within the skeletal muscle fibers has been extensively studied.

sAnk1.5 is one of the small isoforms of Ankyrin1, selectively expressed in striated muscles.

Ankyrin1 is a member of the ankyrin superfamily, which is composed by modular proteins that play a role as adapter proteins between the integral membrane proteins and the cortical cytoskeleton. This superfamily includes three genes: *ANK1* (also known as *ANKR*), first characterized in erythrocytes[63], *ANK2* (also known as *ANKB*), first characterized in brain[64], and *ANK3* (also known as *ANKG*) discovered in node of Ranvier and in epithelial cells[65,66].

These three canonical ankyrins share a common structural organization, with four structural domains (Fig.12):

1. NH_2- terminal region, whose role is to allow the bind to integral membrane proteins; this domain is composed of 24 ANK repeats (24 copies of 33 repeats) folded into four subdomains, each composed by six repeats[67];
2. a central spectrin-binding domain, a 64-kDa domain, whose role is critical for the binding to the cytoskeleton;
3. a death domain, composed approximately of 90 amino acid, whose role is still unknown; moreover, death domains are implicated in homo- or heteromeric interaction with other death domains and, for this reason, it is possible that in particular cellular contests this ankyrin domain might mediate ankyrin homo- or heterodimes;
4. C-terminal regulatory domain that regulates the binding activity of the other domains.

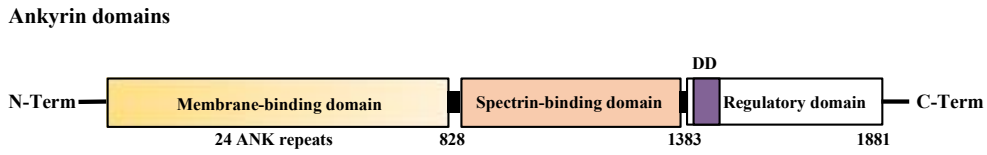

Figure 12: Schematic representation of ankyrin proteins domains. The protein contains 24 ANK repeats at N-terminal region to allow the binding with the integral membrane proteins; a spectrin-binding domain for the binding to the cortical cytoskeleton; a death domain (DD) whose role is still unknown; a regulatory domain at C-terminal region which regulate the binding activity of the other domains. The image was adapted from Lux, 2015[68].

Beyond the three canonical ankyrins (190-220kDa), alternative splicing events, consisting both in domains deletion or insertion, essentially related to the C-terminal region, generate additional isoforms, expressed in tissue and developmental specific manner[69,70]. The size of these spliced variants ranges between 26kDa to 480kDa, and it is possible to divide them into small and giant isoforms[65,69,71,72,73]. In skeletal muscle, tissue specific small isoforms (≈ 20kDa) of Ank1 have been identified. These small isoforms lack both the membrane binding domain and the spectrin-binding domain, while they retain the last 82 aa of the large Ank1 isoform. Through their NH_2 terminal region,

which contains an hydrophobic sequence, they are anchored on the sarcoplasmic reticulum membrane, where they localizes in correspondence of the M band and, at lesser extent, of the Z disks of the sarcomere[59,60,61]. The transcription of these small muscle isoforms is driven by an alternative promoter present between exons 39 and 40 of the *ANK1* gene (Fig. 10), which is active only in striated muscle tissue. Five small isoforms of *ANK1* gene were identified: sAnk1.5, sAnk1.6, sAnk1.7, sAnk1.8, sAnk1.9, even if sAnk1.5 is the most abundant isoforms present in skeletal muscle[16] (Fig.13).

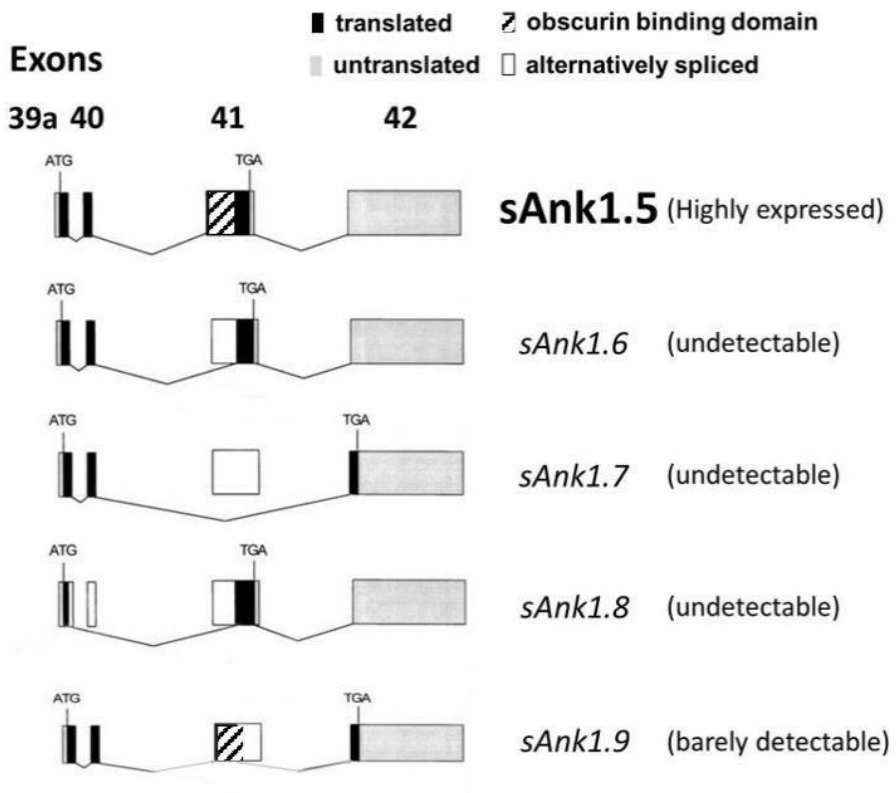

Figure 13: Muscle-specific small isoforms of Ank1. All small isoforms include the exon 39a, codifying the N-terminal region, which is responsible for the insertion of the proteins in the sarcoplasmic reticulum membrane. Only sAnk1.5 and sAnk1.9 share the Obscurin-binding domain, encoded by the exon 41, and their levels are detectable in skeletal muscle. The image was adapted from Gallagher and Forget, 1998[61].

sAnk1.5 is a 17kDa protein, whose structure is composed by a N-terminal Transmembrane domain (TM) and a cytosolic tail[16,59,71]. Through its transmembrane domain, sAnk1.5 localizes on sarcoplasmic reticulum membrane, in particular in correspondence of M-band and, less extend, Z-

disk[59]. This protein is expressed in early stage of development: before birth, sAnk1.5 can be detected in correspondence of the Z disk, while after birth sAnk1.5 is mainly localized in correspondence of the M band. The C-terminal region of sAnk1.5 contains a sequence of 76 amino acids, first characterized in *ANK3* gene[74,75] which is highly conserved in the genome of human, mice and rats, and that is known as Obscurin Binding Domain (OBD). This domain allows the direct interaction between sAnk1.5 and obscurin[76]. Hybridization and pull-down experiments identified two different sites on the COOH-terminal region of obscurin (aa 6231-6262 and aa 6324-6355) able to interact with sAnk1.5. Moreover, experiments performed on skeletal muscle cells transfected with sAnk1.5 protein mutated in specific residues of the OBD domain, showed a mislocalization of mutated sAnk1.5, due to the inability of the mutated protein to bind obscurin. The interaction between sAnk1.5 and obscurin was further confirmed by immunofluorescence experiments[15,77] (Fig.14). In agreement with these results, immunofluorescence signal of sAnk1.5 appeared largely diffused in skeletal muscle fibers of obscurin knock out mouse[17,78].

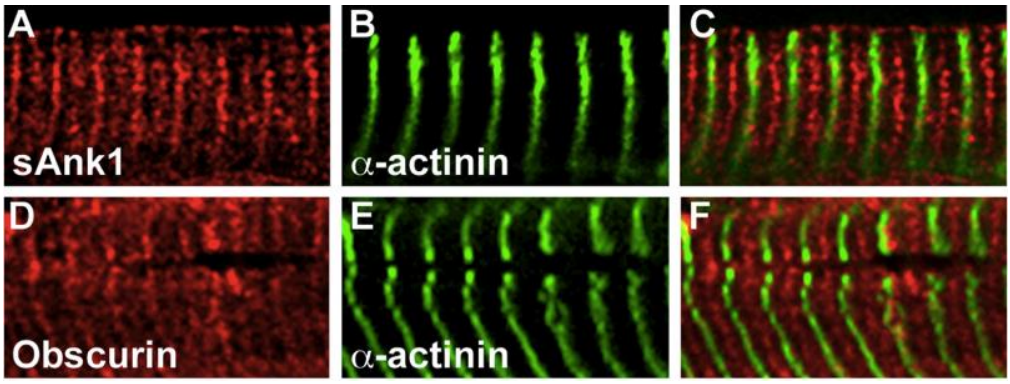

Figure 14: Immunofluorescence experiment performed on longitudinal section of EDL muscle. α-actinin antibody was used to detect Z-disks (panels B and E). Both sAnk1.5 signal (panel A) and Obscurin signal (panel D) were located on the M-bands and less on the Z-disks. Panels C and F represent the merge of α-actinin signal with those of sAnk1.5 and Obscurin, respectively, indicating their colocalization. The image was adapted from Giacomello et al., 2015[77].

To date, the interaction between sAnk1.5 and obscurin is the only known molecular connection that is responsible for tethering the sarcoplasmic reticulum around the contractile apparatus (Fig.15).

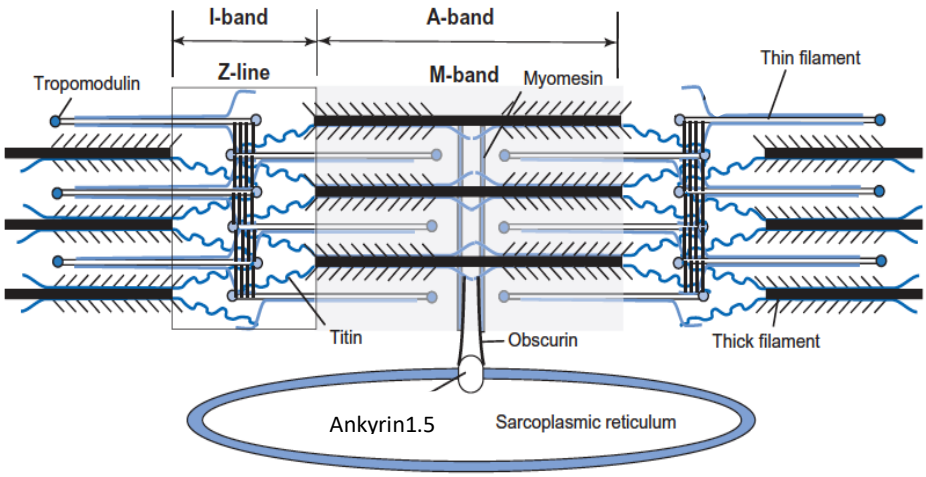

Figure 15: Representative model of interaction existing between Obscurin and sAnk1.5 protein at M-band and Z-disk. This molecular "bridge" is critical to assemble the longitudinal sarcoplasmic reticulum around the contractile apparatus. The image was adapted from Feher, 2017[21].

The importance of this molecular bridge has been further confirmed by the characterization of sAnk1.5 and Obscurin knockout mouse models.

In skeletal muscle of sAnk1.5 knock out mice a significant reduction of l-SR volume was reported in adult mice (Fig.16). Moreover, in aged mice, l-SR volume reduction was accompanied by several structural damages, such as tubular aggregates, contractures and mitochondria and/or triads misplacing[79]. Interestingly, l-SR volume reduction was also observed in skeletal muscle fibers of Obscurin knock out mice[17], further underlying the importance of sAnk1.5/Obscurin interaction in preserving the physiological volume and integrity of the l-SR.

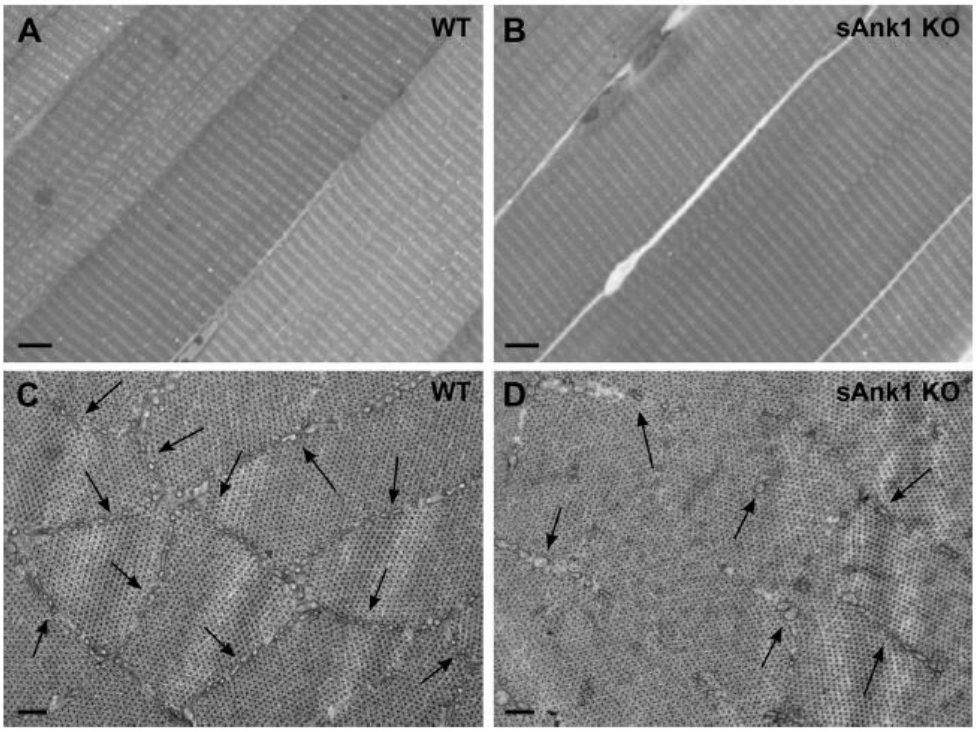

Figure 16: Characterization of sAnk1.5 knock out mice. Longitudinal section of EDL muscle indicates the same structural architecture of sAnk1.5 KO mice muscle compared to wild type (A and B). Cross section of sAnk1.5 KO mice EDL shows a reduction of sarcoplasmic reticulum volume, visible as vesicles and tubules between the myofibrils and indicate by the arrows, compared to EDL of WT mice. The image was adapted from Giacomello et al., 2015[77].

2. Aim of thesis work

In the last decade, genome wide association studies (GWAS) identified several SNPs associated with Type 2 Diabetes (T2D). In particular, in the *ANK1* locus, a high number of SNPs associated to T2D susceptibility have been identified. However, the majority of these SNPs are localized within introns or in regions without known regulatory activities. Interestingly, two independent GWAS studies identified a T2D-associated SNP (rs508419) in the sequence of the internal promoter of the *ANK1* gene, responsible for muscle specific expression of sAnk1.5. The C/C variant of this SNP determines an increased activity of the promoter resulting in increased sAnk1.5 mRNA and protein levels in the skeletal muscle of individuals carrying the C/C genotype, compared to those carrying the T/T one.

The aim of this work was to investigate the actual involvement of sAnk1.5 overexpression in Type 2 Diabetes susceptibility. To this end, we generated a transgenic mouse model where sAnk1.5 was selectively overexpressed in skeletal muscle. We thus monitored glucose and insulin tolerance in transgenic mice over a period of twelve months. In addition, to unveil whether sAnk1.5 overexpression might be associated to T2D susceptibility, we also analyzed glucose and insulin tolerance in transgenic mice fed with a High Fat Diet for twelve weeks.

3. Experimental procedures

3.1 Animal treatment

For this work C57 BL/6J mice were used. They were housed in a controlled environment, with standard condition of temperature (21-25°C) and humidity (50-60%), with a dark-light cycle of 12 hours. Mice had free access to food and water, as reported in the directive 2010/63/EU of the European Parliament and the Council of 22 September 2010 on the protection of animals used for scientific purpose. Mice were sacrificed by occipital-cervical dislocation, as reported in the D.lgs n°26/2014.

MLC-sAnk1.5 transgene was cloned in a pMEX-MLC plasmid in our laboratory. It contains the coding sequence of the murine sAnk1.5, with the untranslated 5' region (714 nucleotides, GenBank accession number: U73972). The sAnk1.5 coding sequence is under the control of the muscle specific myosin light chain promoter (MLC)[80]. The transgenic mice (MLC-sAnk1.5 $Tg^{+/-}$) were generated by the facility of the University of Nanjing, China. Both transgenic and wild type mice (not carrier sibling mice), as control, were then sent to Siena by Dr. Huimei Chen. To expand our colony, we crossed transgenic mice to obtain MLC-sAnk1.5 $Tg^{+/+}$ mice and wild type mice, to obtain the wild type controls. Both wild type and transgenic male mice used for the scientific procedures were 2-6-10 and 12 months old.

3.2 Animal genotyping

3.2.1 DNA extraction

A little piece of mouse tail (<2mm) was taken from anesthetized weaned pups (about 25-days of age). The procedure below was performed with Puregene Core Kit A (Qiagen, Hilden, Germany). Samples were incubated overnight at 55°C in 300 µl of Cell Lysis Solution and 3 µl of Proteinase K enzyme. The day after the enzymatic digestion, 100 µl of Protein Precipitation solution were

added to the samples, vortexed for 20 seconds and centrifuged for 3 minutes at 16000g, in order to precipitate protein components. The resultant supernatants were collected in new tubes. 300µl of Isopropanol were added to the supernatants, samples were inverted 30 times and then centrifuged for 1 minute at 16000g to precipitate the DNA. The supernatants were discarded and the pellets were resuspended in 300µl of Ethanol 70%, vortexed for 5 seconds and centrifuged for 1 minute at 16000g. The supernatants were discarded and the pellets were left under the chemical hood, approximately for 30 minutes, to allow ethanol evaporation. At the end, the DNA were resuspended in 40µl of RNAse/DNAse-free water and heated for 15 minutes at 55° to facilitate their solubilization. DNA concentration was detected by Nanodrop system (Thermo Scientific, Waltham, Massachusetts, USA) and samples were diluted to the final concentration of 20ng/µl.

3.2.2 Qualitative Polymerase Chain Reaction

For mice genotyping, three independent PCR reactions were performed on each DNA sample. Each reaction needs a specific couple of primers, which amplify a certain transgene region (Table 1). Mice were considered transgenic, if each one of the three PCR reactions was positive for the amplicons.

Couple of primers	Name	Sequences (5'->3')	Expected band size	Amplificated region
1	sAnk1.5 Tg-Fw1	CAAGTGAACCGTCCAATCCA	385 bp	MLC Promoter and sAnk1.5 CDS
	sAnk1.5 Tg-Rev1	TGTGGAGATCCAGTTTCTCATTC		
2	sAnk1.5 Tg- Fw2	CAGATGAACAGGGCAACATTG	399 bp	sAnk1.5 CDS and PolyA
	sAnk1.5 Tg-Rev2	TCCCATTCATCAGTTCCATAG		
3	sAnk1.5 Tg-Fw3	ATAGTGCCTTGACTAGAGATC	387 bp	PolyA and MLC Enhancer
	sAnk1.5 Tg-Rev3	GAACCAAAGCATCGACCAGT		

Table 1: Sequences of three couples of primers for sAnk1.5 transgene genotyping

The DNAs were amplified with a master mix containing 2.5µl of Buffer 10X, 2.5µl of dNTPs (stock 2mM), 1µl of each primer (stock 10µM), 0.25 µl of Dream-Taq DNA polymerase (stock 5U/µl), 5 µl of DNA (20ng/µl) and water

to the final volume of 25µl. Cycle times, temperatures and the number of cycles of the amplification program are reported in the Table 2.

Temperature (°C)	Duration	±Tmp/cycle	Cycles
95	5 min		
98	30 sec		20
62	30 sec	-0,5°C	
72	45 sec		
98	30 sec		20
52	30 sec		
72	45 sec		
72	5 min		

Table 2: Amplification program for sAnk1.5 transgene

3.2.3 Agarose gel electrophoresis

PCR reaction products were resolved by electrophoresis run in a 2% agarose gel, dissolved in TAE buffer (Tris-acetate-EDTA 40mM Tris, 20mM acetic acid, 1mM EDTA, pH 8.3). 1µl of SYBR Safe DNA Gel Stain (Invitrogen, Carlsbad, California, USA) per 10mL of agarose gel was added to detect the bands at the end of the run. Before loading, 5µl of loading Buffer 6X (0.25% Bromophenol blue; 0.25% Xylene cyanol; 30% glycerol) were added to each sample. The electrophoretic migration was performed in horizontal electrophoresis chamber (Bio-Rad, Hercules, California, USA), for about 30minutes at constant voltage of 130V, using an Electrophoresis Power Supply (EPS 600, Amersham Pharmacia Biotech, Little Chalfont, UK). At the end of migration, PCR amplification products were visualized by UV transilluminator (220-310 nm) (BioRad, GelDOC1000) and the image was captured by a filter Polaroid BX-600 and thermal paper.

The molecular weight of amplification products was evaluated by comparison with a standard of fragments of known size (Gene Ruler 100bp, Thermo Scientific).

3.2.4 Real Time Polymerase Chain reaction

To discriminate mice carrying MLC-sAnk1.5 Tg $^{+/-}$ genotype from mice carrying MLC-sAnk1.5 Tg $^{+/+}$ genotype, quantitative PCR was needed: therefore, 1ng of DNA was used for Real Time PCR reaction. Each DNA sample (1ng/µl) was resuspended with 0.6µl of forward and 0.6µl of reverse primers (stock 10µM), 10µl of Fast SYBR Green Master Mix (stock 10X, Applied Biosystems, Thermo Fisher Scientific) and water to the final volume of 20µl. This mix was prepared to analyze each sample in triplicate. GAPDH was used for the normalization. The quantitative PCR was performed on Applied Biosystems StepOne Real-Time PCR System. Primers sequences, temperatures, duration and number of cycles of the amplification program are reported in the Table 3-4. Based on recorded cycle thresholds, quantification of transgene expression relative to a reference sample was performed by ΔΔCt method[81].

Step	Temperature (°C)	Duration	Cycles
Polymerase activation	95	20 sec	
Denaturation	95	3 sec	40
Annealing/Extend	60	30 sec	

Table 3: Amplification program for sAnk1.5 transgene Real Time PCR

Primers	Sequences (5'->3')	Annealing region
Ank1.5 Transgene Fw	GAGGAGATCCTTCTTTTGTTCCA	MLC Promoter
Ank1.5 Transgene Rev	GGACGTGGTGACCCACCTG	sAnk1.5 region
GAPDH Fw	CCAGAATGGGAAGCTTGTC	
GAPDH Rev	TCTCGCTCCTGGAAGATGGT	

Table 4: Primer sequences of sAnk1.5 transgene and GAPDH for Real Time PCR

3.2.5 Evaluation of mRNA levels

Gastrocnemius muscles were excised from MLC-sAnk1.5 $Tg^{+/+}$, MLC-sAnk1.5 $Tg^{+/-}$ and wild type mice and the RNA extraction was performed by miRNeasy Mini Kit (Qiagen, Hilden, Germany). Muscles were weighted to add 700µl of Qiazol/100mg of muscle.

Samples were homogenized by Tissue Ruptor, with three strokes of five seconds each, rigorously in ice to avoid the samples overheating. The lysates were leaved for 5 minutes at room temperature. Then, 140µl of chloroform were added, the cap tube closed and the samples were shaken vigorously for 15 seconds. After 2-3 minutes at resting condition at room temperature, the samples were centrifuged for 15 minutes at 4°C at 12000g. Following this centrifugation, the homogenates stratified in two phases: the aqueous one, on the upper side, which contain the RNA partition, and the organic one, in the lower side, which contain DNA, proteins and other debris materials. The aqueous phase was collected in a new 1.5mL tube. 350µl of 70% ethanol were added and the samples were vortexed. 700µl of sample at a time were transferred in RNeasy Mini Spin Columns to be centrifuged for 15seconds at 12000g at room temperature. The flow-through was discarded and 700µl of RWT Buffer were added to the columns and then centrifuged at room temperature for 15 seconds at 12000g. The flow-through was discarded, 500µl of RPE Buffer were added and the columns were centrifuged at room temperature for 15 seconds at 12000g. The washing step with RPE Buffer was then repeated. The columns were centrifuged to the highest speed for 1 minute, to eliminate the RPE buffer residues. The RNeasy Mini Spin Columns were placed in a new 1.5mL tube, 40µl of RNase-free water were added directly onto the filters of the columns. To elute RNA, the columns were centrifuged at room temperature, at 12000g for 1.30 minute.

RNA samples were loaded on a 1.2% agarose gel for horizontal electrophoresis migration to verify RNA integrity. 2µl of each RNA sample were mixed with 8µl of RNase free water and 2µl 6X DNA Loading Dye (Thermo Fisher Scientific, Waltham, Massachusetts, USA). The electrophoresis run was performed in horizontal electrophoresis chamber (Bio-Rad), previously cleaned

with RNAse Zap solution (Thermo Fisher Scientific, Waltham, Massachusetts, USA), at 70V for about 45minutes. The size of RNAs fragments were evaluated by comparison with a ladder with bands of known length (Gene Ruler 1kb, Thermo Scientific).

To perform the Real Time PCR, RNAs were retro transcribed to obtain cDNA. Retro transcription was performed with the Promega kit and consisted into two steps: 1µg of each RNA sample was resuspended with 0.5µg of Random primer/µg RNA and RNAse-free water to reach a final volume of 15µl and incubated at 70°C for 5minutes; then, M-MLV Buffer 5X, dNTPs 20mM, RNasin 40U/µl, M-MLV Retro transcriptase 200U/µl and RNAse-free water were added to each sample, to achieve a final volume of 25µl, and the solution was incubated for 1hours at 42°C. The quantity of reagents needed for the mix for one sample are reported in Table 5.

Reagents	Quantity for 1 Sample	
0,25 µg RNA	4 µl	STEP1 5minutes 70°C
0,5µg Random Primers/ µg RNA	1 µl	
H_2O	10 µl	
M-MLV Buffer 5X	5 µl	STEP 2 1 hour 42°C
dNTPs 20mM	0,625 µl	
Rnasin 40U/µl	0,5 µl	
M-MLV RT 200U/µl	1 µl	
H_2O	2,875 µl	

Table 5: Composition of the mix for cDNA retro-transcription

Amplification of β-actin by PCR was performed on cDNAs to verify the correct retro transcription of the samples. 2µl of cDNA were amplified in a final volume of 25µl, using 2.5µl of Buffer 10X, 2.5µl of dNTPs (stock 2mM), 1µl of both forward and reverse primers for β-actin (stock 10µM), 0.25 µl of

Dream-Taq (stock 5U/µl). Temperature, duration and number of cycles of the program of amplification reaction are reported in the Table 6.

Temperature (°C)	Duration	Cycles
95	5 min	
95	30 sec	30
54	30 sec	
72	45 sec	
72	10 min	
4	HOLD	

Table 6: Amplification program for β-actin.

The amplified products of the PCR reactions were resolved by horizontal electrophoresis migration on 2% agarose gel dissolved in TAE, for 30minutes at constant voltage of 130V. The size of amplification products was evaluated by comparison with Gene Ruler 100bp ladder (Thermo Fisher Scientific).

Quantitative Real Time PCR was performed on cDNAs obtained. All samples were analyzed in triplicate using Fast SYBR Green PCR fluorescence technology (Applied Biosystems, Foster City, California, USA), and normalized using β-actin as an endogenous control. Primer concentrations used in the mix were 0.3 µM for both β-actin primers, 0.3 µM and 0.05µM for reverse and forward primers, respectively, of sAnk1.5 transgene. The expression ratio of the gene of interest was calculated using the Comparative CT method (ΔΔCT) of relative quantification.

The primers sequences used are reported in Table 7.

Name	Forward Sequences (5'->3')	Reverse Sequences (5'->3')
β-actin	GATGAGATTGGCATGGCTTT	CACCTTCACCGTTCCAGTTT
m-Ank1.5	CTGGTGCTGTTAGGCTTCTTC	GTTCCTGGTGGATGTGCTTC

Table 7: Primer sequences for Real Time PCR

3.3 Evaluation of protein levels

3.3.1 Tissue lysate preparation

Gastrocnemius muscles were excised from three-months-old male mice with MLC-sAnk1.5 $Tg^{-/-}$ and MLC-sAnk1.5 $Tg^{+/+}$ genotypes. The muscles, excised in ice, were immediately frozen in liquid nitrogen and stored at -80°C until the use. All the steps below were performed on ice to avoid protein degradation. The frozen muscles were lysed in RIPA Buffer (50nM Tris-HCl ph7.4; 1% NP40; 0.25% sodium deoxicolate; 150mM NaCl; 1mM EDTA), supplemented with 1mM PMSF (phenylmethylsulfonyl fluoride) and protease inhibitor cocktail (2μg/mL aprotinin, leupeptin, chymostatin, pepstatin A, antipain) and then homogenized with Tissue Ruptor with two strokes of 5 seconds each. Homogenized samples were left for 1 hour at 4° in movement to allow digestion and then centrifuged for 15 minutes at 4° at 11000g to precipitate non-lysate material. The supernatant, rich in proteins, was recovered and transferred in a new tube.

3.3.2 Measurement of protein concentration

Proteins concentration was determined through the Bradford assay. This is a colorimetric assay based on the absorbance shift of the dye Comassie Brilliant Blue G-250 when added with different protein concentrations. The absorbance of the sample at 595 nm is measured and the protein concentration is determined in reference to a standard curve of know concertation of bovine serum albumin (BSA, Sigma Aldrich, St. Louis, Missouri, USA).

10µl of each samples was diluted with 20µl (1:3) or 90µl (1:10) of bi-distillated water, respectively, and 10µl of these dilutions were added to 790µl of bi-distillated water and 200µl of Bradford solution (Protein Assay Dye Reagent concentration kit, BioRad). The optical density of the entire solution was read to the spectrophotometer Ultrospec 2100 pro UV/visible (Amersham Bioscience, Little Chalfont, UK), using a wavelength of 595nm. Protein concentration (µg/µl) of each sample was obtained by the average between the OD of the two measurements.

3.3.3 SDS-Page electrophoresis

Muscle lysates were resolved with a run on a polyacrylamide gel, with the addition of sodium dodecyl sulphate (SDS-Page), whose function is due to its denaturant action, which confers a negative charge to the protein. In this way, the natural charge of the protein became negligible and the ratio weight/charge of denatured polypeptides became the same for different protein. As result, the run of the protein will be only based on molecular weight.

The electrophoresis migration was performed on 10% acrylamide homemade gel (Table 8) or on 4-12% gradient PreCast gel (Invitrogen, Thermo Fisher Scientific). 10µg of each lysate were mixed to Sample Buffer 4X (250mM Tris-HCl pH 6.8, SDS 2%, glycerol 40%, β-mercaptoethanol 20%, bromophenol blue 0.016%) and H_2O to a final volume of 20µl, heated at 95°C for 5 minutes and then loaded on the gel. The homemade 10% gels were run in TGS 1X running buffer (stock TG10X: 25mM Tris-HCl ph8.3, 1.44% glycine) plus 0.1% SDS, at 25mA, for 2 hours. The 4-12% precast gels were run in NuPAGE MES buffer 1X (50mM MES, 50mM Tris, 0.1% SDS, 1mM EDTA, pH7.3), at 200V for 30 minutes. In order to identify proteins of interest by their molecular weight, gel was also loaded with a ladder (Precision Plus Protein Standards, Dual color, BIORAD) containing proteins of known molecular weights.

Stacking 4%		Running 10%	
Acrylamide/Bis-acrylamide, 30% solution SIGMA ALDRICH	600 µl	Acrylamide/Bis-acrylamide, 30% solution SIGMA ALDRICH	3,3 mL
0,5M Tris-HCl pH 6.8 BIORAD	1,25 mL	3M Tris-HCl pH 8.8 BIORAD	2,5 mL
SDS 10% (Sodium Dodecyl Sulphate) BIORAD	50 µl	SDS 10% (Sodium Dodecyl Sulphate) BIORAD	100 µl
APS 1,5% (Ammonium Persulphate,98%) SIGMA ALDRICH	250 µl	APS 1,5% (Ammonium Persulphate,98%) SIGMA ALDRICH	500 µl
TEMED (N,N,N1,N1-Tetra Methylenthylenediamide) BIORAD	3,75 µl	TEMED (N,N,N1,N1-Tetra Methylenthylenediamide) BIORAD	5 µl
H_2O	2,8 mL	H_2O	3,55 mL

Table 8: Polyacrylamide gel 10% composition for SDS PAGE. The gel is composed by an upper part, the stacking, with a fixed concentration of acrylamide (4%), and by a lower part, the running, whose concentration depends on the molecular weight of the protein to analyze.

3.3.4 Western Blot

Proteins separated by SDS-PAGE were transferred onto nitrocellulose blotting membrane (GE Healtcare Life Science, Little Chalfont, UK). The transferring was performed in TG1X buffer (stock TG10X: 25mM Tris-HCl ph8.3, 1.44% glycine) with the addition of 0.1% SDS and 15% methanol, at 400mA, at 4°C for 2 hours. To evaluate the transfer quality, the nitrocellulose membrane was stained with Ponceau red (0.2% Red Ponceau, 0.2% Trichloroacetic acid TCA) for 5 minutes and rinsed rapidly with distillated water to remove the excess. The image of stained transferred proteins was acquired with ChemiDoc technology (Biorad). The membrane was incubated with a blocking solution composed of non-fat dried milk 5% dissolved in TBS-T (Tris-Buffered Saline and TWEEN 20: 20mM Tris-HCl, pH7.4, 150mM NaCl, 0.1% TWEEN 20), for one hour at room temperature, in order to mask non-specific sites, which can interact with the primary antibodies. The membranes were incubated overnight at 4° with the primary antibodies, diluted in TBS-T solution with 5% non-fat milk. The antibodies used were:

1- rabbit antibody for sAnk1.5 III bleed (1:1000)[16]
2- mouse antibody for GAPDH (Clone GA1R, 1mg/ml, Thermo Fisher Scientific, 1:1000)

The day after, the membranes were rinsed three times for 10 minutes with 0.5% non-fat milk TBS-T and then incubated for one hour with secondary antibodies at room temperature. The secondary antibodies (anti- rabbit/mouse IgG, GE Healtcare), specific for the constant fragments of the primary antibodies and conjugated to the horseradish peroxidase, were diluted 1:3000 in 5% milk TBS-T. Following the membranes were rinsed three times with 0.5% non-fat milk TBS-T for 10 minutes. The bands relative to the binding of the antibody to the proteins of interest were detected and acquired through the release of a luminescent signal detectable with a luminescence counter (Chemidoc, BIORAD). This signal was obtained through the incubation of the membranes with Enhanced Chemi Luminescence (ECL, Biorad) solution, which reacted with the horseradish peroxidase.

3.4 Evaluation of protein localization

3.4.1 Isolation and culture of single fibers

Flexor Digitorum Brevis (FDB) muscles were excised from wild type, MLC-sAnk1.5 $Tg^{+/+}$, and MLC-$Tg^{+/+}$ mice and incubated in a myorelaxing solution for 10 minutes on ice. A collagenase solution composed of Collagenase (SIGMA C0130 0,4%W/V) + Tyrode (SIGMA T2145) + 10% Fetal Bovine Serum (FBS) (SIGMA 12103C) was prepared and filtered. Tyrode buffer and myorelaxing solution composition are reported in Table 9.

The muscles were transferred in a tube with 3mL of collagenase solution and incubated previously at 4° for 1 hour and then at 37°, 5% CO_2 for 1:30 hour. Meanwhile, Lab-tek 8wells (Sarstedt) culture chambers were coated with laminin (SIGMA, St. Louis, Missouri, USA) and left in the incubator at 37°C, 5% CO_2. After collagen digestion, the muscles were rinsed three times with 3mL of different solutions: Tyrode for 10 minutes at 37°C, 5% CO_2; Tyrode + FBS 10% for 10 minutes at 37°C, 5% CO_2; Tyrode + FBS 10% +

Penicillin/Streptomycin 1% for 10 minutes at 37°C, 5% CO_2. After each washing step, the solution was removed but not completely, in order to keep the muscle wet. The FDB were put in a sterile dish (35mm) to carefully remove the tendons and skin residues, trying to avoid damaging fibers. Muscle fibers were definitively separated tipping up and down with progressively smaller pipettes (5mL, 2mL and 1mL).

The suspensions containing the fibers were tip up and down to be homogeneous, distributed in the laminin coated Lab-tek and left overnight at 37°C, 5% CO_2.

Tyrode Buffer (pH7.4) SIGMA T2145		**Myorelaxing solution (pH7.8)**	
$CaCl_2$	**0,2 g/l**	**KCl**	**0,1 M**
$MgCl_2$	**0,1 g/l**	**EGTA**	**5 mM**
KCl	**0,2 g/l**	**$MgCl_2$**	**5 mM**
Na_2HPO_4	**8 g/l**	**BDM**	**3 mM**
Glucose	**1 g/l**	**DTT**	**0,25 mM**
To add:		**Hystidine**	**10mM**
$NaHCO_3$	**1 g/l**		
HEPES (SIGMA H1016)	**6 g/l**		

Table 9: Composition of Tyrode and myorelaxing solutions

3.4.2 Immunofluorescence

In order to evaluate the localization of sAnk1.5 transgene protein, the day after immunofluorescence assay was performed on FDB fibers.

The medium was aspirated and two rapid washing steps were performed with PBS 1X. The fibers were incubated with paraformaldehyde 3% + sucrose 2% for 7 minutes at room temperature. After a washing step in PBS 1X+ BSA 0,2%, the fibers were permeabilized with Hepes-Triton10X Buffer for 3 minutes at room temperature. Following, they were incubated in PBS 1X+BSA 0,2%+goat serum 5% blocking solution for 90 minutes and then incubated with

the primary antibody solution overnight at 4°C. α-Ank1 (Aviva Systems Biology) and α-actinin (EA-53, Sigma-Aldrich) primary antibodies were respectively diluted 1:1000 and 1:500 in PBS 1X+ BSA 0,2%. The day after, the fibers were rinsed two times with PBS 1X + BSA 0,2% for 10 minutes and incubated for 1 hour at room temperature with the secondary antibody solution. Cy3 conjugated secondary anti mouse (red) and Alex Fluor 488 (Invitrogen) conjugated anti rabbit secondary antibodies were both diluted 1:5000 in PBS 1X + BSA 0,2%. Following a rapid wash, the fibers were observed by confocal microscope (Zeiss LSM800) and the images were acquired.

3.5 Investigation on mice glucose tolerance

3.5.1 Intraperitoneal Glucose Tolerance Test

Intraperitoneal Glucose Tolerance Tests (IPGTTs) were performed on MLC-sAnk1.5Tg$^{+/+}$ and wild type mice at 2-6-10-12 months of age. The mice were fasted for 17 hours (from 5 pm to 10 am, approximately) and housed individually in cages containing a grid to avoid any contact with litter and excrements. Following fasting, mice were weighted and 10µl of a solution of 20% D-glucose (SIGMA) per gram of mouse weight was injected intraperitoneally, corresponding to a final administration of 2g/kg of glucose. To measure glucose levels in blood, a small drop of blood was collected on the glucose strip of a glucometer (OGC care, Biochemical System International, Arezzo, Italy) after making a cut at the tip of the mouse tail. Blood glucose concentration was measured before the injection (t0) and 30, 60, 120 and 180 minutes after the injection.

3.5.2 Intraperitoneal Insulin Tolerance Test

Intraperitoneal Insulin Tolerance Tests (IPITT) were performed on MLC-sAnk1.5Tg$^{+/+}$ and wild type mice. After 5 hours of fasting (from 10 am to 15 pm), the mice were weighed and 10µl insulin solution per grams of mouse weight was injected intraperitoneally, corresponding to a final administration

of 1U/kg. To measure glucose levels in blood, a small drop of blood was collected on the glucose strip of a glucometer (OGC care, Biochemical System International, Arezzo, Italy) after making a cut at the tip of the mouse tail. Blood glucose concentration was measured before the injection (t0) and 15, 30, 60, 90 and 150 minutes after the injection.

3.6 Statistical analysis

The optical density of bands from immunoblotting experiments were quantified as reported by Taylor and colleagues[82], using "Imagen Lab software, 2017". The statistical analysis was performed using Student's T-test, with a threshold of significance of $p \leq 0.05$.

4. Results

4.1 Generation and expansion of MLC-sAnk1.5$^{+/+}$ mouse colony

The entire coding sequence of murine sAnk1.5, including the 5'-untranslated region (714 nucleotides, GenBank number U73972) was cloned in the pMEX plasmid (6757 nucleotides), which contained the 1500-bp fragment of the muscle-specific rat myosin light chain promoter (MLC), 840-bp fragment of SV40 polyA, and 900-bp fragment of the end of MLC1f/3f gene, which acts as an enhancer[80]. This construct (MLC-sAnk1.5 transgene) was used by a facility of Nanjing University, China, to generate transgenic mice carrying a single copy of the transgene (MLC-sAnk1.5 Tg$^{+/-}$ mice). Five MLC-sAnk1.5 Tg$^{+/-}$ mice (3 males and 2 females) and five wild type mice (WT, 2 males and 3 females) of 8-12 weeks of age were intercrossed in the animal house of University of Siena to expand both transgenic and sibling WT mouse colonies. Pups' genotype was established by qualitative PCR on genomic DNA, extracted from the tail-tip of weanling mice, by using three different pairs of primers, designed to amplify three distinct regions of the transgene. The DNA extracted from the tail-tip of the founder mice, generated in China, (F0) were used as positive and negative controls (Fig.17A). Mice were considered transgenic only when all the three amplicons were detected (Fig. 17B). MLC-sAnk1.5 Tg$^{+/-}$ mice were fertile, and presented an undistinguishable phenotype compared to WT mice.

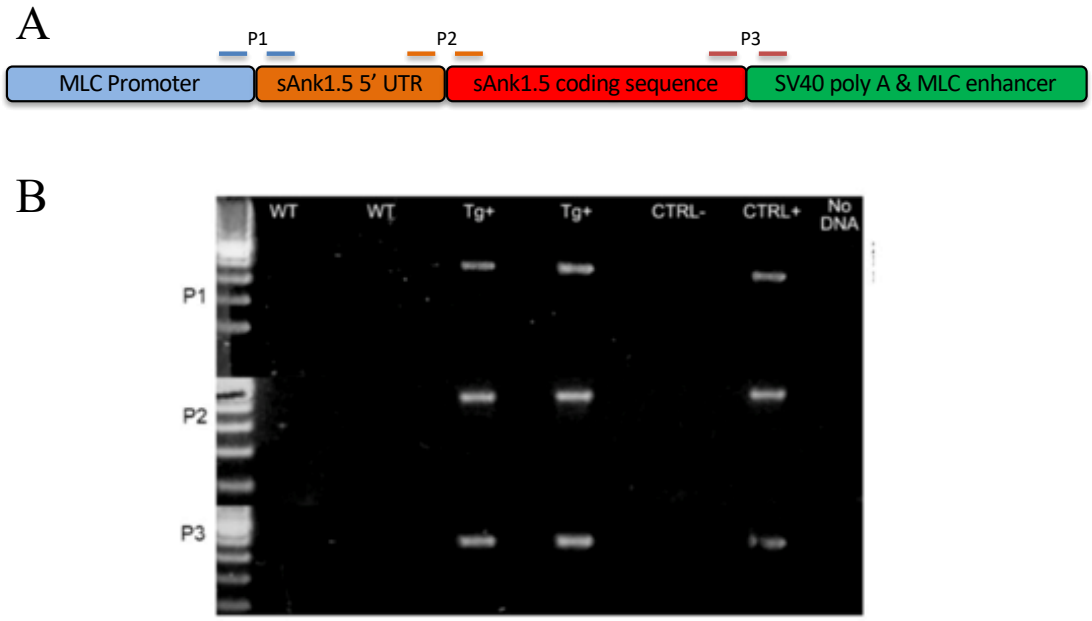

Figure 17: Representative qualitative PCR of mice genotyping A) Schematic representation of the MLC-sAnk1.5 transgene. Red lines on top of the cartoon represent the region of the transgene amplified by the three different pair of primers (P1, P2, P3) used for genotyping. B) Representative genotyping using three distinct pair of primers that amplify distinct regions of the transgene. The presence of the amplicon band for each couple indicates mice genotype. DNA from founder mice (F0) were used as negative and positive controls.

We, then, intercrossed MLC-sAnk1.5 $Tg^{+/-}$ mice to generate a mouse colony carrying two copies of the transgene. WT and MLC-sAnk1.5 $Tg^{+/+}$ pups from such breeders were generated at the expected frequency of one out of four newborns mice. The presence of two copies of the transgene (MLC-sAnk1.5 $Tg^{+/+}$ mice) and the absence of the transgene (sibling WT mice) were evaluated by quantitative PCR on genomic DNA, using a pair of primer specifically designed to amplify the joining region between the MLC promoter and the 5' untranslated region of sAnk1.5 transcript (Fig 18A). As reported in Figure 18B, this experimental approach allowed us to discriminate between pups carrying one copy of the transgene and those carrying two copies. In fact, following application of the ΔΔCt method, using samples from MLC-sAnk1.5 $Tg^{+/-}$ founder mice as internal reference, MLC-sAnk1.5 $Tg^{+/+}$ mice were identified when transgenic sequence was 2-fold increased compared to MLC-sAnk1.5 $Tg^{+/-}$ mice. No signal above basal threshold was detected in samples from wild type mice, indicating the absence of the transgene. All the following

experiments were performed on MLC-sAnk1.5 $Tg^{+/+}$ male mice, using wild type sibling mice as control, unless otherwise indicated.

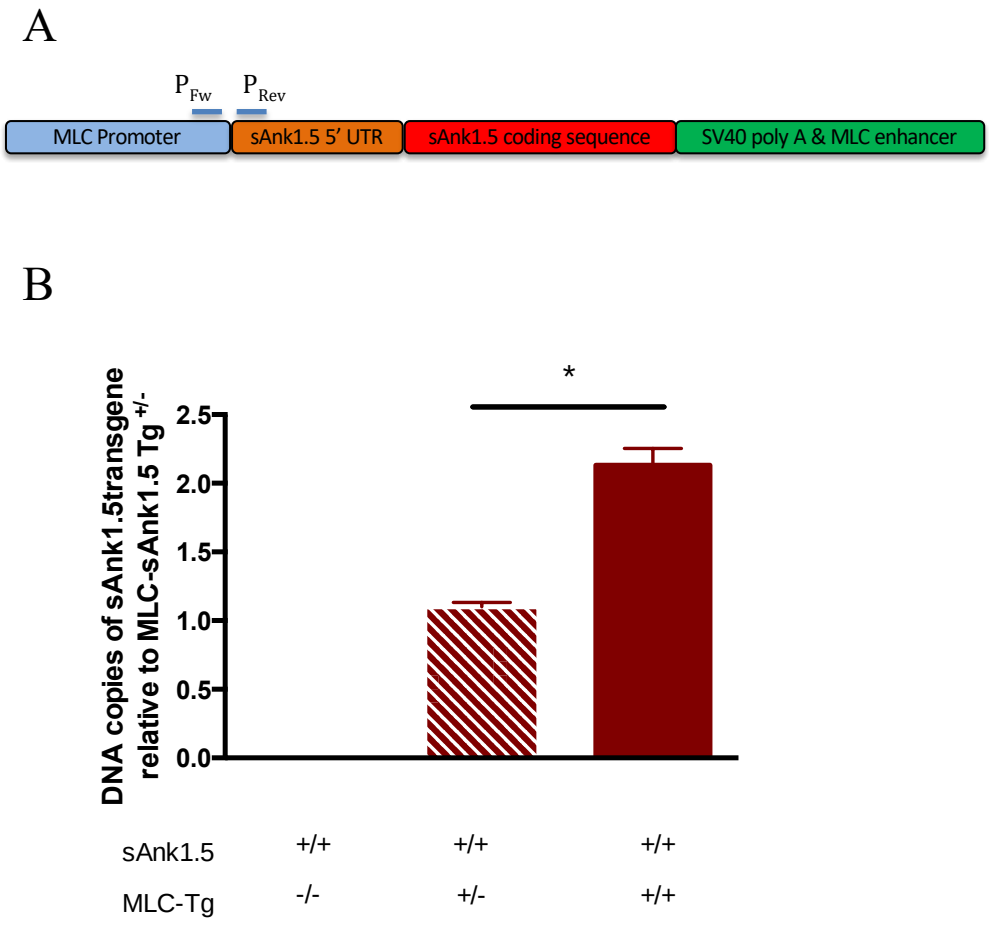

Figure 18: **Representative graph of genotyping of WT and MLC-sAnk1.5 $Tg^{+/+}$ mice born from MLC-sAnk1.5 $Tg^{+/-}$ breeders.** Genomic region recognized by pair of primers used in these experiments are reported in the panel A. Genomic DNA of MLC-sAnk1.5 $Tg^{+/-}$ founder mice was used as internal reference and arbitrarily set as 1 (panel B). MLC-sAnk1.5 $Tg^{+/+}$ mice have been identified through the 2-fold increase of transgenic sequence, compared to the MLC-sAnk1.5 $Tg^{+/-}$ mice. In parallel, no signals for transgenic sequence were detected in the WT samples. P value is calculated by Student's t-test; * $p<0,05$.

4.2 Characterization of sAnk1.5 mRNA and protein levels in transgenic mice

Once defined the genotype, the transgenic mice were characterized also by the mRNA and protein levels of sAnk1.5. sAnk1.5 mRNA expression levels in skeletal muscles of MLC-sAnk1.5 $Tg^{+/-}$, MLC-sAnk1.5 $Tg^{+/+}$ and WT mice, revealed an increase by about 15 folds and 30 folds respectively, compared to wild type mice, as shown in Figure 19.

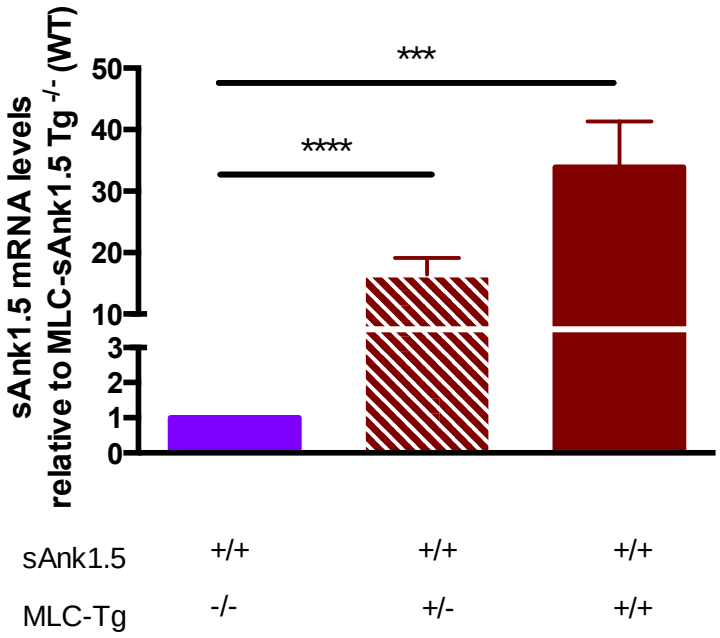

Figure 19: Histogram representation of sAnk1.5 mRNA levels in gastrocnemius muscle of WT, MLC-sAnk1.5 $Tg^{+/-}$ and MLC-sAnk1.5 $Tg^{+/+}$ mice. Expression of sAnk1.5 mRNA relative to WT is reported as the mean ± SD of 4 experiments. sAnk1.5 mRNA levels in MLC-sAnk1.5 $Tg^{+/-}$ and MLC-sAnk1.5 $Tg^{+/+}$ mice were increased respectively 15 folds and 30 folds, compared to WT mice. P values are calculated by Student's t-test; *** P<0.001, **** P<0.0001.

In parallel, sAnk1.5 protein levels were performed with western blot experiments on total protein lysates obtained from different skeletal muscles, namely gastrocnemius, *extensor digitorum longus* (EDL) and soleus.

10µg of muscle lysates were separated in a 4-12% Precast Gel, blotted onto nitrocellulose filter, and sAnk1.5 signal revealed by using a specific anti-sAnk1.5 antibody[16].

As shown in Fig 20 A and B, we observed an increase of 43% of sAnk1.5 in the gastrocnemius muscle of MLC-sAnk1.5 $Tg^{+/+}$ mice compared to wild type. Similarly, in EDL muscle of MLC-sAnk1.5 $Tg^{+/+}$ mice, we detected a 52% increase of sAnk1.5 protein levels (Fig. 20 C and D).

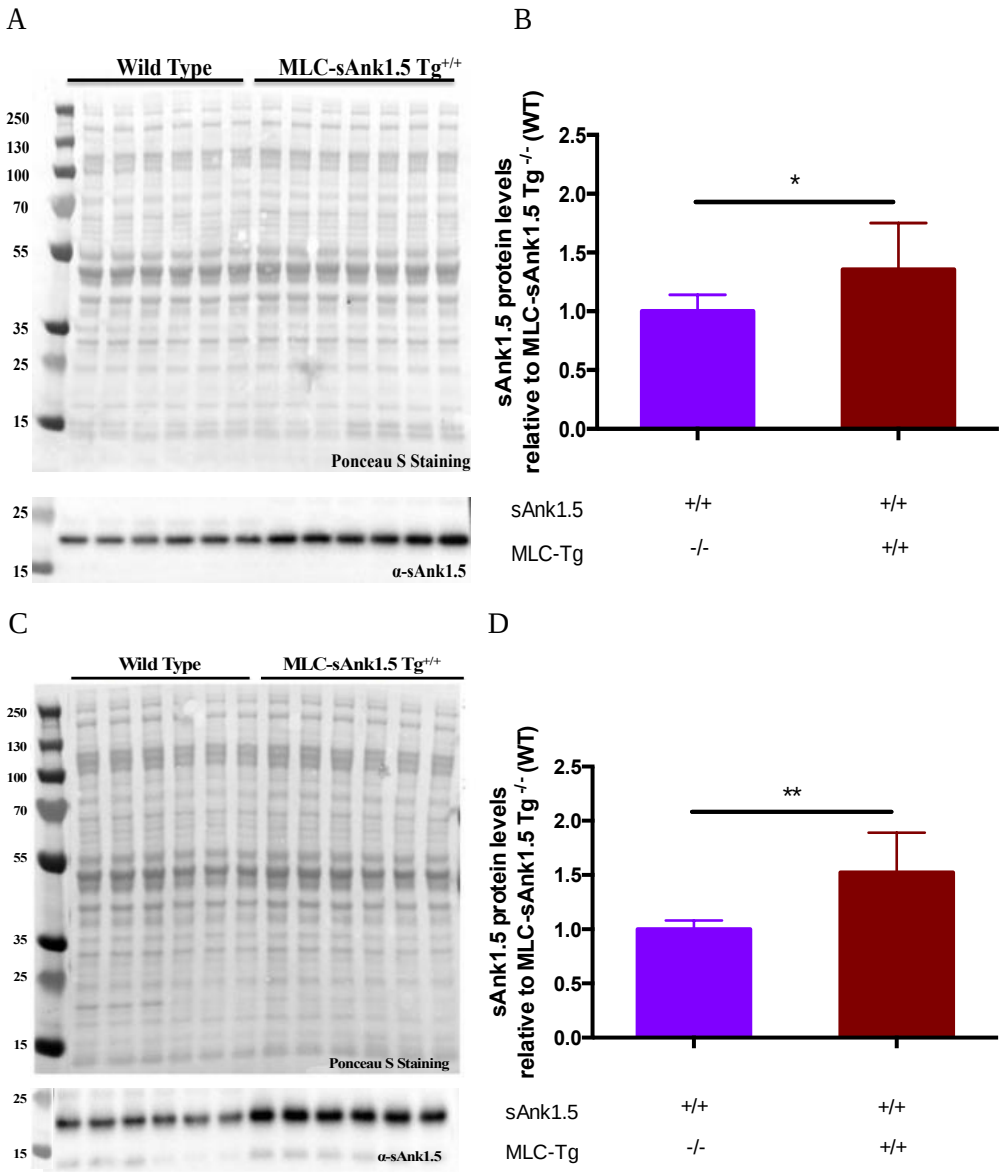

Figure 20: Representative image of SDS-PAGE and Western blot analysis performed on total lysates prepared from the gastrocnemius (A) and EDL (C) muscle lysates of transgenic and WT mice. Ponceau-red staining of nitrocellulose membrane following the protein transfer was used to normalize the optical density of sAnk1.5 signals. The histograms (B and D) report the mean ± S.D. of expression sAnk1.5 protein relative to the WT. A significative increase of sAnk1.5 protein in gastrocnemius and EDL transgenic muscles, 43% and 52% respectively, was observed compared to the muscles of WT mice. P value was calculated by Student's t-test; * P=0.0170; ** P= 0.0020.

In contrast, western blot analysis on total protein lysates from soleus muscle did not reveal any difference in sAnk1.5 protein levels between MLC-sAnk1.5 $Tg^{+/+}$ and WT mice (Fig. 21).

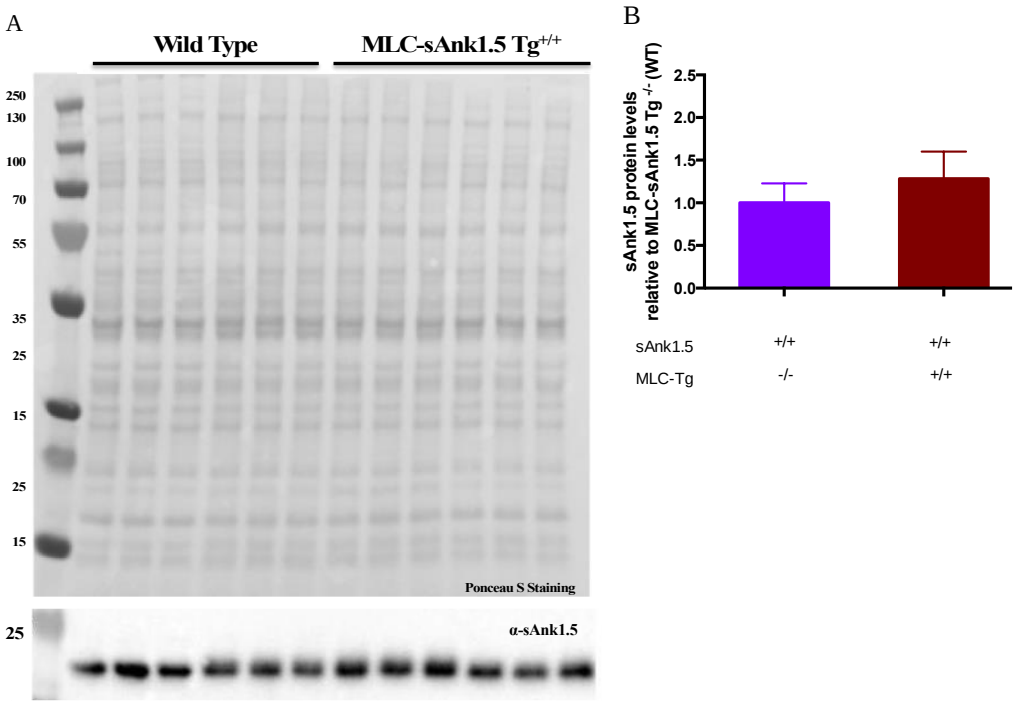

Figure 21: Representative image of SDS-PAGE and Western blot analysis performed on total lysates prepared from the soleus muscle lysates of transgenic and WT mice. Ponceau-red staining of nitrocellulose membrane following the protein transfer was used to normalize the optical density of sAnk1.5 signals. No differences were detected in sAnk1.5 protein levels between WT and transgenic soleus muscles. The histograms report the mean ± S.D. of expression sAnk1.5 protein relative to the WT.

To verify the striated muscle specific expression of the MLC-sAnk1.5 transgene, western blot analysis was also performed on total protein lysates prepared from spleen, brain, liver, lung, skeletal muscle and heart of MLC-sAnk1.5 $Tg^{+/+}$ mice. As shown in Fig.22A, the band relative to sAnk1.5 was detected in total protein lysates from skeletal muscle, but not in those prepared from any other analyzed organs.

To better assess transgene expression in cardiac and skeletal muscle tissue, total protein lysates from heart, liver and gastrocnemius prepared from MLC-sAnk1.5 $Tg^{+/+}$ mice, were analyzed against heart, liver and gastrocnemius total protein lysates prepared from sAnk1.5$^{-/-}$ // MLC-sAnk1.5 $Tg^{+/+}$ mice. These latter transgenic mouse line does not express endogenous sAnk1.5, but does express sAnk1.5 transgene, thus representing a suitable mouse model to discriminate between endogenous and transgenic sAnk1.5 protein expression.

As shown in Figure 22 B and D, the expression levels of sAnk1.5 in gastrocnemius was, as expected, about 50% increased in both MLC-sAnk1.5

$Tg^{+/+}$ and sAnk1.5$^{-/-}$//MLC-sAnk1.5 $Tg^{+/+}$, compared to WT mice. In contrast, sAnk1.5 protein levels were comparable in the heart of all three mouse lines analyzed (Fig. 22 B and D).

To verify the correct localization of transgenic sAnk1.5, we performed immunofluorescence experiments on sAnk1.5$^{-/-}$//MLC-sAnk1.5 $Tg^{+/+}$ *tibialis anterior* (TA) fibers. As showed in Figure 22C, transgenic sAnk1.5 protein signal was detected in correspondence of M-band, and lesser extent at Z-disk, as described for the endogenous protein[59].

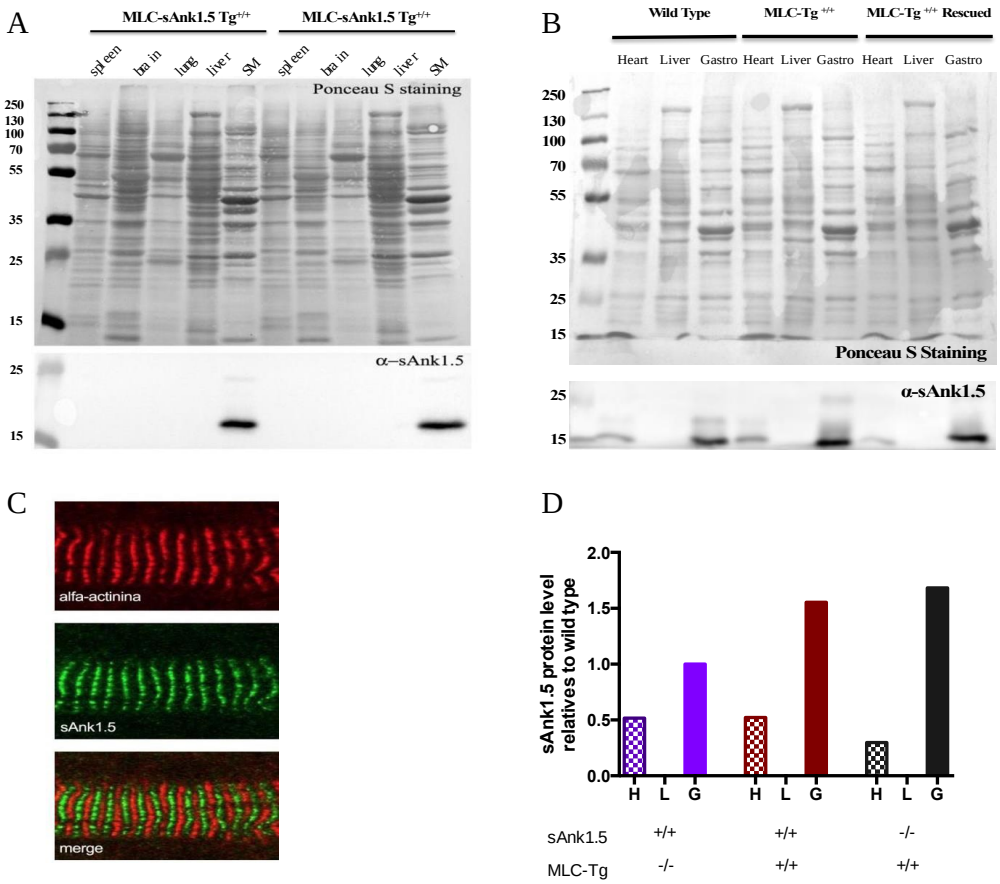

Figure 22: Representative image of SDS-PAGE and Western blot performed on total protein lysates prepared from spleen, brain, lung, liver and skeletal and cardiac muscles (A and B). Ponceau-red staining of nitrocellulose membrane following the protein transfer was used to normalize the optical density of sAnk1.5 signals. D) The histograms report the mean ± S.D. of expression sAnk1.5 protein in sAnk1.5$^{-/-}$//MLC-sAnk1.5 $Tg^{+/+}$ and MLC-sAnk1.5 $Tg^{+/+}$ relative to the WT. sAnk1.5 protein is detected in skeletal muscles, although a weaker band can be observed in total heart protein lysates. C) Immunofluorescence experiments on *tibialis anterior* fibers isolated from a sAnk1.5$^{-/-}$ // MLC-sAnk1.5 $Tg^{+/+}$ mouse. The anti-sAnk1.5 antibody recognized its target in correspondence of M-band and, at lesser extent, of Z-disk. Scale bar: 5μ

4.3 Analysis of glucose and insulin tolerance in transgenic mice

To verify whether increased levels of sAnk1.5 might be associated to a pre-diabetic or diabetic phenotypes, glucose tolerance was monitored over a period of twelve months.

Intra-peritoneal glucose tolerance test (IPGTT) was performed on 2 months old MLC-sAnk1.5Tg$^{+/+}$ and wild type mice. After 17 hours fasting, the glycaemia curves, obtained with measurements of blood glucose concentration at 0, 30, 60, 120, 180 minutes, revealed that the blood glucose levels of transgenic mice, at any time of recording, were similar to those of wild type mice (Fig.23A). Accordingly, the area under the curve parameter (A.U.C.), which is an indicator of the overall glucose disposal during the test, was not different between transgenic and wild type mice (Fig.23B).

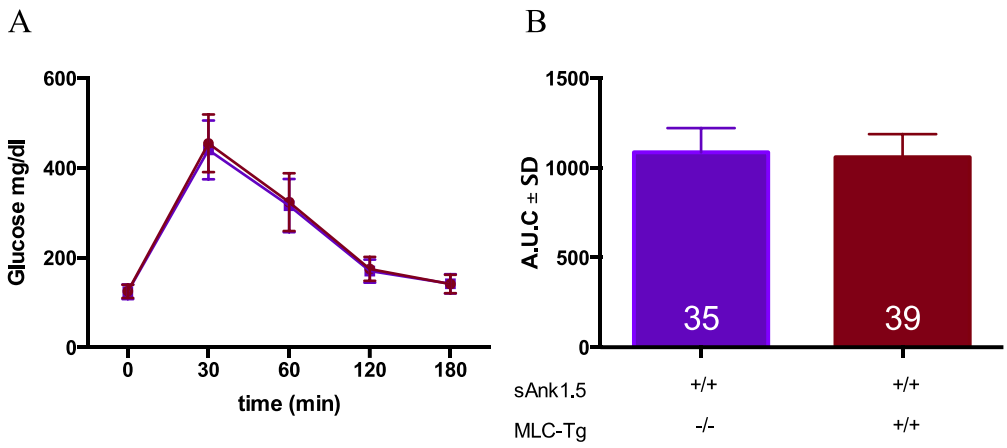

Figure 23: IPGTT experiment performed on 2-months old WT and transgenic mice. A) Following 17-hours fasting, glucose (2g/kg) was administered via intra-peritoneal injection and blood glucose concentration was measured at 0, 30, 60, 120, 180 minutes following the administration. B) The histograms represent of the areas under the curves (A.U.C.) means± S.D. values.

T2D is a multifactorial disease, as its onset relies on both genetic and environmental cues. Among the environmental causes there is ageing: in fact, older people are more prone to develop this pathology[83]. We thus monitored glucose tolerance in MLC-sAnk1.5 Tg$^{+/+}$ and wild type mice at 7-10-12-months of age. The glucose curves obtained following IPGTT performed at 7-

10-12-months of age showed that MLC-sAnk1.5 $Tg^{+/+}$ and WT mice displayed a comparable glucose tolerance at any age (Fig.24A, C, E). These results were also confirmed by calculating A.U.C. values from the glycemic curves (Fig.24 B, D, F).

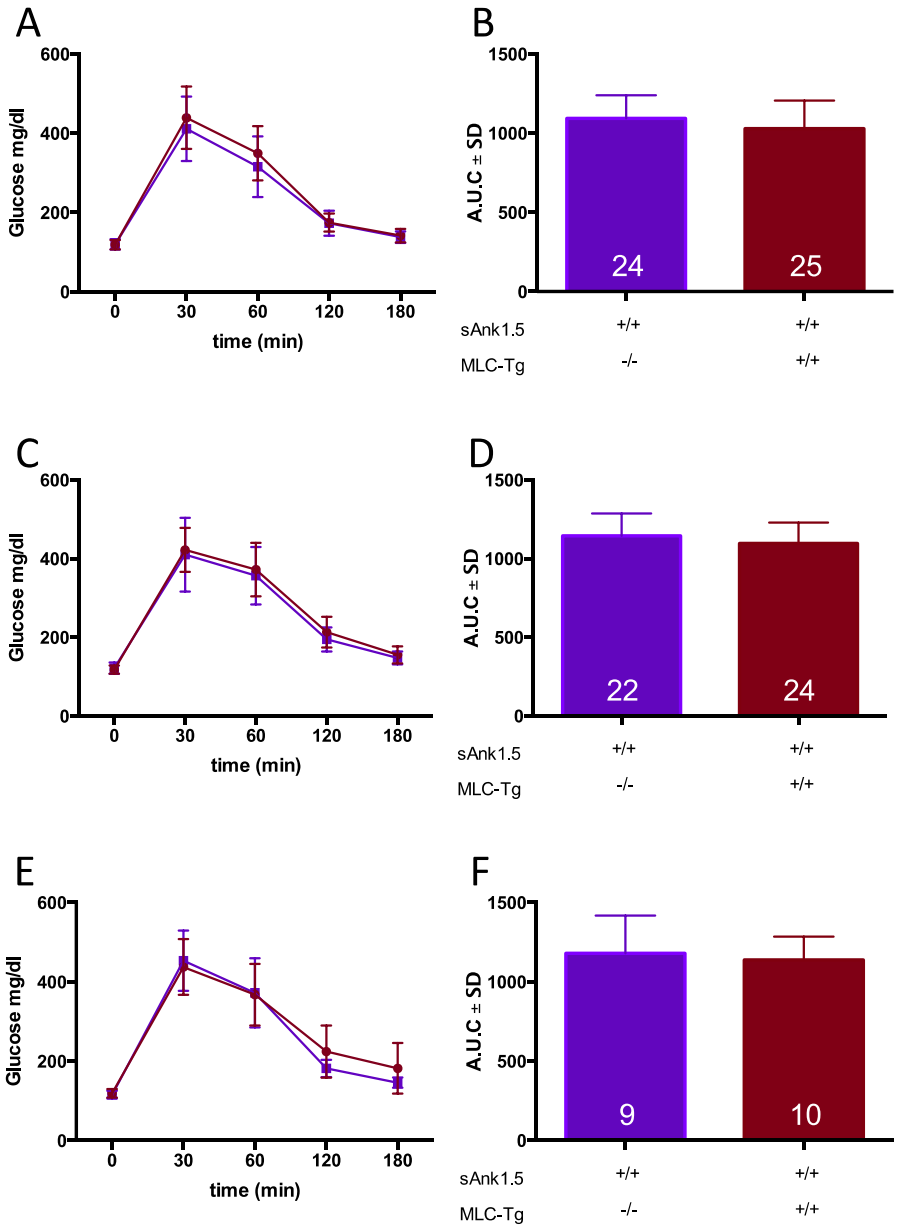

Figure 24: IPGTT experiments performed on transgenic mice 7- (panel A), 10- (panel C) and 12- (panel E) months old. Following 17-hours fasting, glucose (2g/kg) was administered via intra-peritoneal injection. Blood glucose concentrations were measured at 0, 30, 60, 120, 180 minutes following the administration. The histograms represent the areas under the curves (A.U.C.) means± S.D. values (panels B, D and F). As shown, transgenic and WT mice did not display any difference in glucose tolerance, at any age analyzed.

In addition, we performed intraperitoneal insulin tolerance test (IPITT) in MLC-sAnk1.5 $Tg^{+/+}$ and wild type 12-months old mice. Accordingly, with the IPGTT experiments, transgenic mice displayed a comparable insulin tolerance with the respect to WT mice (Fig.25).

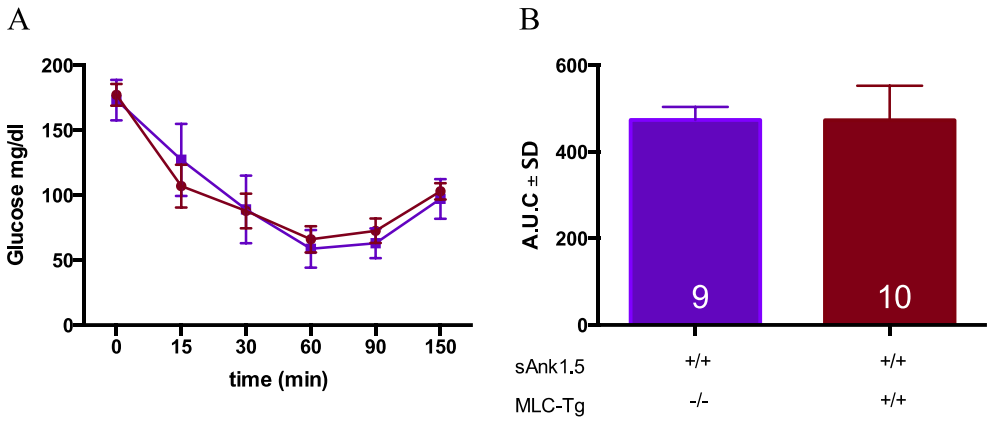

Figure 25: IPITT experiments performed on transgenic mice 12-months old. Following 5-hours fasting, insulin (1U/kg) was administered via intra-peritoneal injection. Blood glucose concentrations were measured at 0, 15, 30, 60, 90, 150 minutes following the administration (panel A) and no difference in insulin tolerance were found between WT and transgenic mice. The histograms represent the areas under the curves (A.U.C.) means± S.D. values (panels B).

4.4 High Fat diet experiments

The obesity is another environmental major risk factor for Type 2 Diabetes onset[83]. Since IPGTT performed on standard fed wild type and MLC-sAnk1.5 $Tg^{+/+}$ mice over a period of 12-months revealed no difference in glucose tolerance, we fed both wild type and MLC-sAnk1.5 $Tg^{+/+}$ mice with a high fat diet to unveil whether sAnk1.5 overexpression might be associated to T2D susceptibility.

To this end, 35 wild type and 39 MLC-sAnk1.5 $Tg^{+/+}$ 2-months old mice were divided into 4 experimental groups and fed with either a standard or high fat diet over a period of 12 weeks.

Before high fat feeding, glucose tolerance test was performed to record the initial glycaemia of all mice. As shown in the Figure 26, glucose tolerance was

comparable between MLC-sAnk1.5 $Tg^{+/+}$ and WT mice, in agreement with previous results.

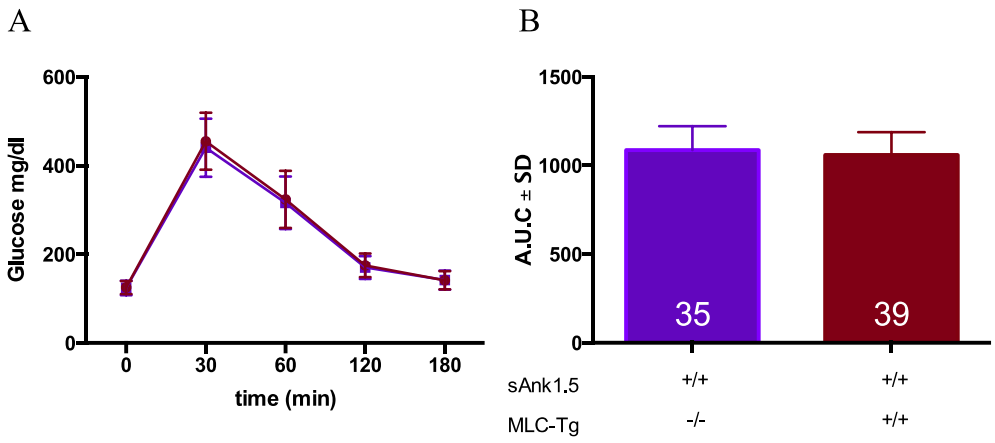

Figure 26: IPGTT experiment at the beginning of high fat diet. Blood glucose concentration levels in transgenic and wild type 2-months old mice before starting the high fat diet protocol (panel A). Following 17-hours fasting, glucose (2g/kg) was administered via intra-peritoneal injection. Blood glucose concentrations were measured at 0, 30, 60, 120, 180 minutes following the administration and no differences were found between WT and transgenic mice. The histograms represent the areas under the curves (A.U.C.) means± S.D. values (panel B).

During the 12 weeks of the protocol, weight gain parameters, the daily food and kilocalories consumption were monitored in all four groups. As shown in Figure 27 A and B, MLC-sAnk1.5 $Tg^{+/+}$ and WT mice displayed comparable weight gain efficiency relative to the specific diet protocol, calculated as a percentage of weight increase with the respect to the body weight measured at the beginning of the diet. MLC-sAnk1.5 $Tg^{+/+}$ mice fed with the high fat diet, moreover, ate around 1.5 grams/day less than those fed with chow diet, and 0.5grams/day more than wild type fed with high fat diet (Fig.27 C and D). These differences mirrored the weekly increase of absolute values of the relative body weight (data not shown) and the values relative to the kilocalories assumption with the different diets, obtained multiplying the daily eaten food with the fuel energy of two different diets (4,74 kcal/g for high fat one and 3,15 kcal/g for standard one) (Fig.27 E and F).

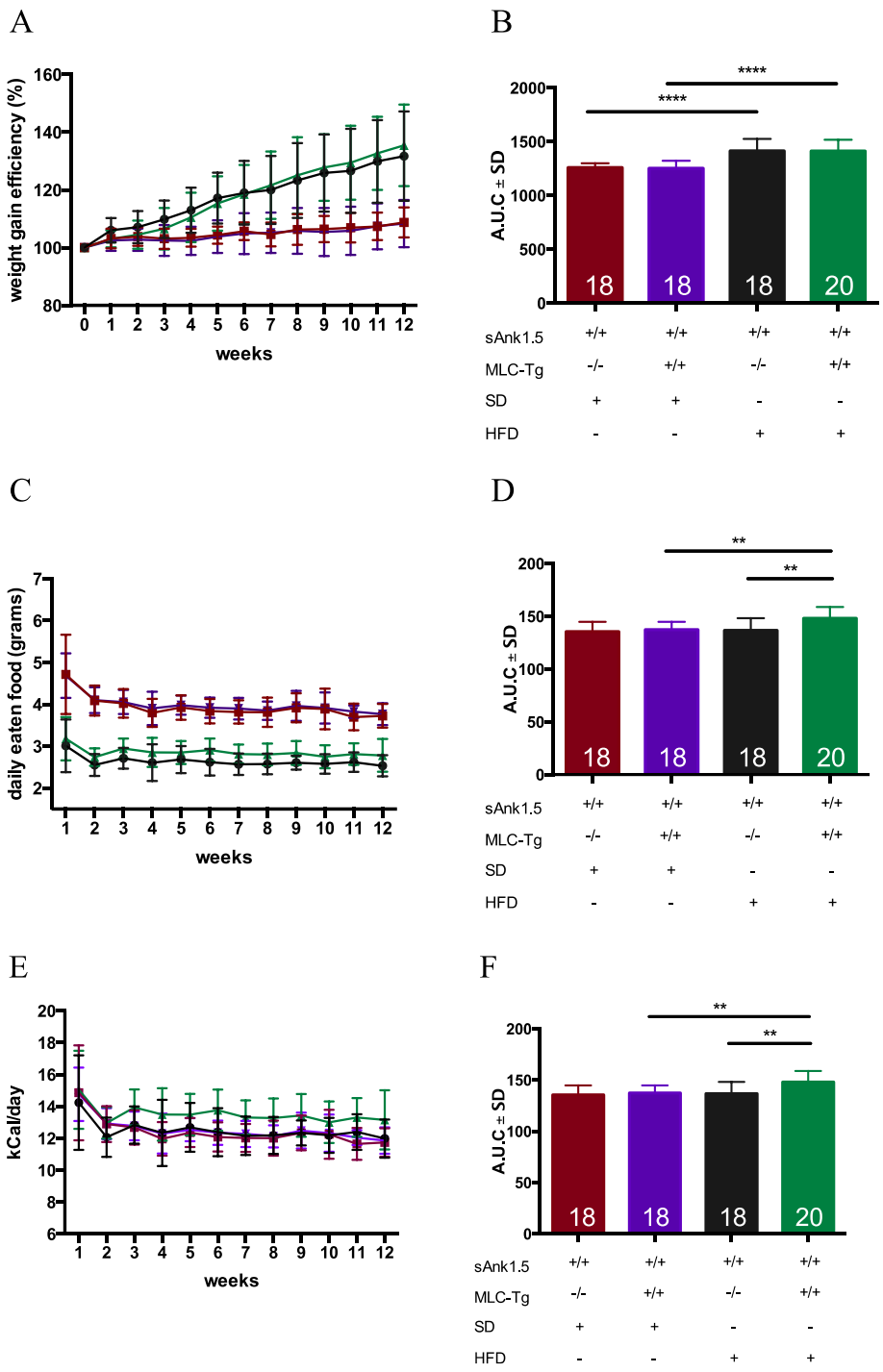

Figure 27: Daily food consumption and weight gain parameters, during 12 weeks of diet protocol. Transgenic and WT mice fed with the high fat diet have a significative increase in weight gain efficiency, with the respect to the mice fed with chow diet (panel A). Moreover, the standard diet fed mice eat 4g/day of food compared to transgenic and WT mice fed with high fat diet, which eat 2.5g/day, approximately (panel C). This difference in the daily food consumption is confirmed by the kilocalories acquired with the different diets (panel E).

The histograms represent the areas under the curves (A.U.C.) means± S.D. values (panels B, D and F). p-values were calculated with Student's T-test. **p<0.1, ****p<0.0001.

Alteration of basal blood glucose concentration is considered as a parameter of pre-diabetic phenotype. We thus measured basal blood glucose levels in standard and high fat fed mice, after 8 and 12 weeks from the beginning of the experiment. Following both 8 and 12 weeks of diet, as expected, blood glucose levels were significantly increased in high fat fed mice compared to genotype-matched standard fed mice. However, no difference between MLC-sAnk1.5 $Tg^{+/+}$ and WT mice fed with either high fat or chow diet were observed (Fig.28).

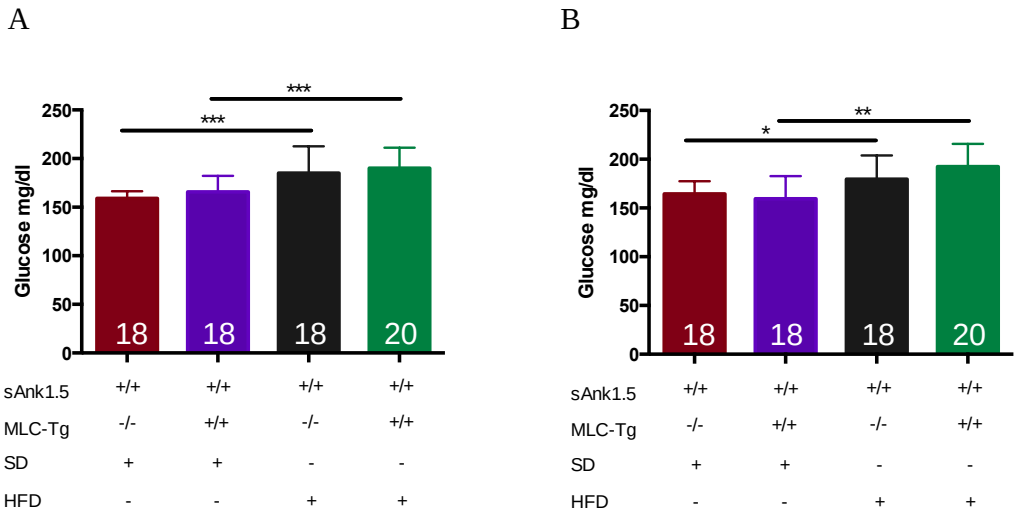

Figure 28: Basal blood glucose levels following both 8- and 12- weeks of high fat diet protocol. The basal blood glucose levels were measured on mice regularly fed. Basal glucose levels were significantly increased in high fat fed mice compared to genotype-matched standard fed mice, both at 8- (panel A) and 12- (panel B) weeks of diet protocol. p-values were calculated with Student's t-test: *p<0.05, **p< 0.001 ***p<0.0001.

Following 12 and 14 weeks of the diet protocol, IPGTT and IPITT, respectively, were performed to evaluate whether sAnk1.5 overexpression might exacerbate the development of a pre-diabetic or diabetic phenotype. As shown in Figure 29, MLC-sAnk1.5 $Tg^{+/+}$ and WT mice fed with high fat diet displayed a significant increase in blood glucose levels at any time of recording after intraperitoneal glucose administration (Fig. 29 A) and a significant reduction in the overall glucose tolerance (Fig. 29 B), with respect to genotype-matched standard fed mice. When the effect of the different diets was compared between MLC-sAnk1.5 $Tg^{+/+}$ and WT mice, we found no difference between the two groups.

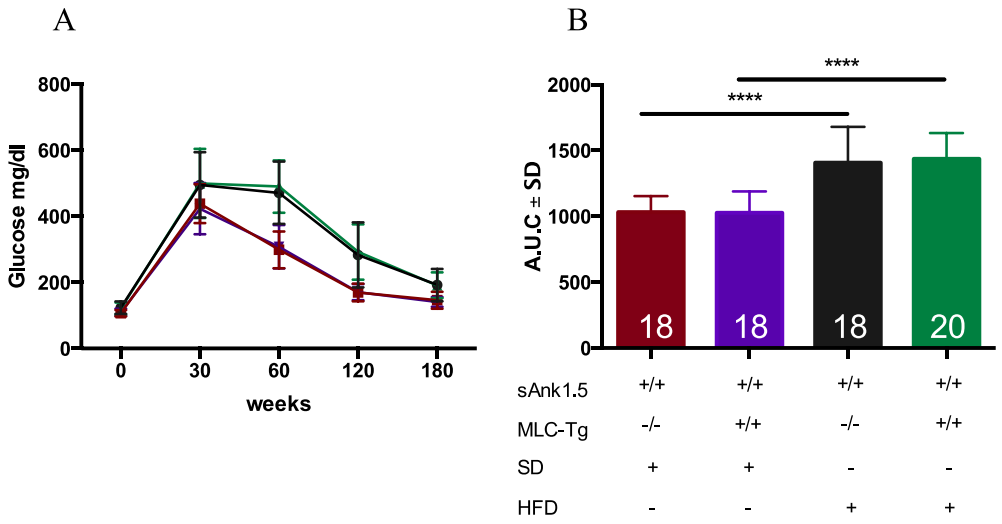

Figure 29: IPGTT performed following of 12 weeks of the diet protocol. Following 17-hours fasting, glucose (2g/kg) was administered via intra-peritoneal injection and blood glucose concentration was measured at 0, 30, 60, 120, 180 minutes following the administration (panel A). The histograms represent the areas under the curves (A.U.C.) means± S.D. values (panel B). As shown in panels A and B, the mice fed with high fat diet have an increase in the glucose intolerance, compared to those fed with standard diet, while no difference were found between WT and transgenic mice fed with the same diets. p-values were calculated with Student's t test: ****$p<0.0001$.

These groups of mice were also tested through IPITT for the ability to respond to insulin stimulus. This experiment was performed two weeks later than the IPGTT. After 5 hours of fasting, glycaemia was measured at 0, 15, 30, 60, 90, 150 minutes after the insulin injection. As shown in Figure 30, high fat fed mice displayed a reduced insulin tolerance compared to standard fed mice. However, no differences in insulin tolerance were found between MLC-sAnk1.5 $Tg^{+/+}$ and WT mice fed with the same diet.

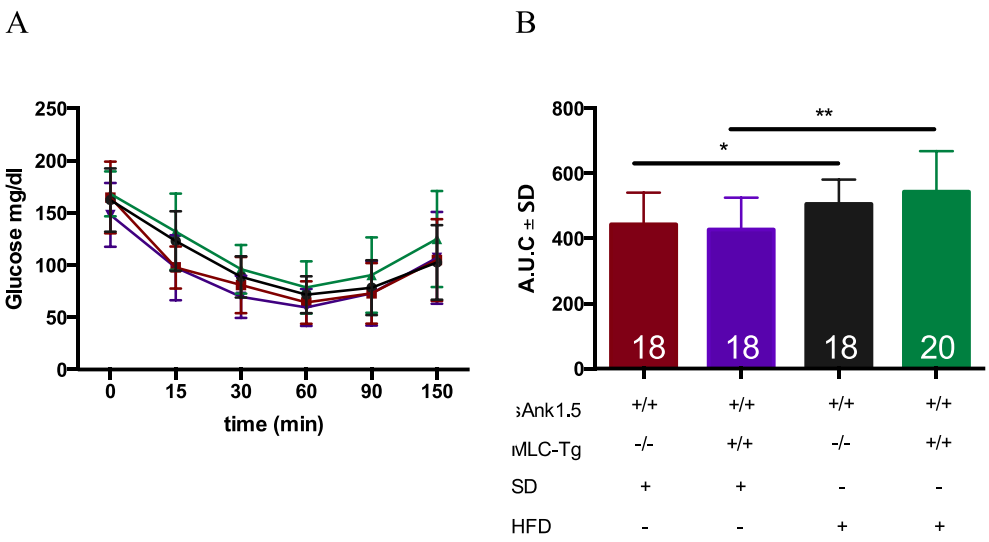

Figure 30: IPITT performed following of 14 weeks of the diet protocol. Following 5-hours fasting, insulin (1U/kg) was administered via intra-peritoneal injection and blood glucose concentration was measured at 0, 15, 30, 60, 90, 120 minutes following the administration (panel A). The histograms represent the areas under the curves (A.U.C.) means± S.D. values (panel B). As shown in panels A and B, only high fat diet fed mice have a reduced insulin tolerance, compared to standard diet fed ones. p-values were calculated with Student's t test: *$p<0.05$, **$p<0.001$.

5. Discussion

sAnk1.5 is a striated muscle-specific protein localized on the l-SR in correspondence of the M band and Z disk of the sarcomere, where interacts with the giant sarcomeric protein Obscurin, generating the only known molecular bridge between the SR and the contractile apparatus[15,16,84], responsible for the proper juxtaposition of the SR around the myofibrils. In addition, sAnk1.5 plays a pivotal role in the maintenance of l-SR volume, thus preserving several physiological and structural aspects of skeletal muscle fibers[77,85,86]. sAnk1.5 transcription is driven by an internal promoter of the *ANK1* gene, which is active only in striated muscle fibers [61].

Genome wide association studies identified several SNPs associated to T2D susceptibility in the ANK1 locus, although the major part of them reside in intronic regions or in regions without a known regulatory activity. Of note, two recent independent GWAS studies identified a new SNP (rs508419) that is localized within the *ANK1* internal promoter. The C/C variant of this SNP has been associated to T2D susceptibility. Interestingly the C/C variant determines an increased activity of the promoter, resulting in higher mRNA and protein levels of sAnk1.5 with respect to those present in the skeletal muscle of individuals carrying the T/T variant, which in turn does not represent a risk allele for T2D susceptibility[54]. These studies suggest that increased protein levels of sAnk1.5 in skeletal muscle may represent a condition that favors the onset of a diabetic phenotype.

To investigate whether sAnk1.5 overexpression in skeletal muscle might be associated to T2D susceptibility, we generated a transgenic mouse model in which the sAnk1.5 coding sequence is under the transcriptional control of the striated muscle specific rat myosin light chain promoter (MLC).

To verify whether this transgenic mouse line represented a suitable model to test the association between sAnk1.5 overexpression and T2D susceptibility, we firstly characterized sAnk1.5 expression pattern. As expected the transgene is expressed only in striated muscle. In particular, transgene expression is by far most abundant in skeletal muscle with respect to cardiac tissue, in agreement with previous observation[80]. In addition, we found that MLC-

sAnk1.5 transgene is preferentially expressed in those muscles characterized by the prevalence of glycolytic fibers (i.e. gastrocnemius and EDL), while its expression is negligible in muscles mainly composed by oxidative fibers (i.e. soleus), in agreement with previous characterization of the expression pattern of the pMEX-MLC plasmid[80]. Surprisingly, sAnk1.5 mRNA levels in skeletal muscles of MLC-sAnk1.5 $Tg^{+/+}$ mice were increased by about 40-folds compared to wild type, in strong contrast with the increase of sAnk1.5 protein of only 1.5 folds. This could be explained by post-translational regulatory mechanisms. Indeed, the correct localization of sAnk1.5 is dependent on its interaction with obscurin and its anchorage at the sarcomeric M-band. When such interaction lacks, due to the absence of obscurin, sAnk1.5 protein is ubiquitinated and then degraded[17]. In our transgenic mouse model, a similar situation may be generated by the excess of sAnk1.5 protein, which saturate all the obscurin binding sites, leaving a conspicuous amount of protein without its binding partner. However, yet unknown post-transcriptional and/or post-translational regulation mechanisms cannot be ruled out.

However, in spite of a 50% increase of sAnk1.5 protein in skeletal muscle of transgenic mice, immunofluorescence experiments indicated that sAnk1.5 is properly localized in correspondence of the M band and Z disks of the sarcomere.

To summarize, the results obtained from the characterization of sAnk1.5 expression pattern in MLC-sAnk1.5 transgenic mice indicate that this mouse line represents a suitable model to study the correlation between increased levels of sAnk1.5 and T2D susceptibility[54,62].

T2D is a multifactorial metabolic disorder characterized by insulin resistance condition, whose pathologic phenotype is an inefficient absorption of blood glucose by insulin responsive tissues, such as skeletal muscle and adipose tissue[87]. In particular, skeletal muscle tissue, due to its mass relative to the entire body weight, is the main tissue involved in glucose clearance from the blood. Indeed, is not uncommon that skeletal muscle dysfunctions result in the onset of systemic metabolic disorders[37,87,88].

We thus initially performed IPGTT on 2-months old wild type and MLC-sAnk1.5 $Tg^{+/+}$ mice, but we did not observe any difference in glucose tolerance

between the two groups. It is known that aging is a risk factor for the onset of T2D[87]. Accordingly, we monitored glucose tolerance of transgenic mice over a period of 12 months. However, also following this analysis, transgenic mice did not show any alteration in both fasting glucose and glucose tolerance. We also performed insulin tolerance test on transgenic mice at 6 and 12 months of age, but also this analysis did not reveal significant differences between transgenic and WT mice. We are currently planning to analyze glucose and insulin tolerance in transgenic mice older than twelve months, because it has been reported that male mice may display a significant deterioration in glucose and insulin tolerance between six and eighteen months of age[89].

Although glucose and insulin tolerance of MLC-sAnk1.5 $Tg^{+/+}$ mice was not affected, at least by twelve months of age, we reasoned that obesity is another environmental major risk factor for the onset of T2D[89]. Accordingly, to better understand whether increased sAnk1.5 protein levels may represent an actual factor associated to T2D susceptibility, we induced an obesity condition in the mice, by feeding them with a high fat diet, in order to force the appearance of pre-diabetic and/or diabetic phenotype. Following the diet protocol, through IPGTT and IPITT experiments, we observed that transgenic and WT mice fed with high fat diet displayed a significant reduction in overall glucose and insulin tolerance, with respect to genotype-matched standard fed diet. These results were also confirmed by basal glucose levels measured at 8- and 12-weeks the high fat diet protocol, indicating that, independently from the diet, transgenic mice seem not to develop any glucose tolerance alteration.

In conclusion, our results seem indicate that sAnk1.5 overexpression does not appear to predispose to a pre-diabetic or diabetic condition in mice.

To date, it is known that sAnk1.5 interacts with SERCA1 pump, present on the sarcoplasm reticulum membrane. sAnk1.5 transmembrane domain, indeed, share a homology with the sequence of sarcolipin and phospholamban, the two most well-known SERCA inhibitors[90,91]. The interaction between sAnk1.5 and SERCA1 seems to regulate SERCA1 activity, reducing Ca^{2+}- affinity of the pump[92]. Since calcium ions activate GLUT4 vesicles trafficking, through the activation of both PKC and CAMKII kinases[37], and sAnk1.5 seems to inhibit SERCA pumps, we would better investigate on the molecular pathways

implicated in the translocation of GSVs from the intracellular storage pools to the plasma membrane.

6. Bibliography

1. Frontera WR, Ochala J. Skeletal Muscle: A Brief Review of Structure and Function. *Behav Genet*. 2015;45(2):183-195. doi:10.1007/s00223-014-9915-y
2. Monesi V. *Istologia*. VI. (Piccin, ed.).; 2012.
3. Krendel M, Mooseker MS. Myosins : Tails (and Heads) of Functional Diversity Myosins : Tails (and Heads) of Myosin Superfamily : Diversity of. *Physiology*. 2006:239-251. doi:10.1152/physiol.00014.2005
4. Rosol M, Lehman W, Craig R, Landis C, Butters C, Tobacman LS. Three-dimensional reconstruction of thin filaments containing mutant tropomyosin. *Biophys J*. 2000;78(2):908-917. doi:10.1016/S0006-3495(00)76648-3
5. Lin BL, Song T, Sadayappan S. Myofilaments: Movers and rulers of the sarcomere. *Compr Physiol*. 2017;7(2):675-692. doi:10.1002/cphy.c160026
6. Milligan RA. Protein-protein interactions in the rigor actomyosin complex. *Proc Natl Acad Sci*. 2002;93(1):21-26. doi:10.1073/pnas.93.1.21
7. Scott W, Stevens J, Binder–Macleod SA. Human Skeletal Muscle Fiber Type Classifications. *Phys Ther*. 2001;81(11):1810-1816. doi:10.1093/ptj/81.11.1810
8. Liu G, Mac Gabhann F, Popel AS. Effects of Fiber Type and Size on the Heterogeneity of Oxygen Distribution in Exercising Skeletal Muscle. *PLoS One*. 2012;7(9). doi:10.1371/journal.pone.0044375
9. Schiaffino S. Fibre types in skeletal muscle: A personal account. *Acta Physiol*. 2010;199(4):451-463. doi:10.1111/j.1748-1716.2010.02130.x
10. Luther PK. The vertebrate muscle Z-disc: Sarcomere anchor for structure and signalling. *J Muscle Res Cell Motil*. 2009;30(5-6):171-185. doi:10.1007/s10974-009-9189-6
11. Gautel M, Djinović-Carugo K. The sarcomeric cytoskeleton: from molecules to motion. *J Exp Biol*. 2016;219(2):135-145. doi:10.1242/jeb.124941
12. Bang ML, Li X, Littlefield R, et al. Nebulin-deficient mice exhibit shorter thin filament lengths and reduced contractile function in skeletal muscle. *J Cell Biol*. 2006;173(6):905-916. doi:10.1083/jcb.200603119
13. Young P, Ehler E, Gautel M. Obscurin, a giant sarcomeric Rho guanine nucleotide exchange factor protein involved in sarcomere assembly. *J Cell Biol*.

2001;154(1):123-136. doi:10.1083/jcb.200102110

14. Bang ML, Centner T, Fornoff F, et al. The complete gene sequence of titin, expression of an unusual ≈700-kDa titin isoform, and its interaction with obscurin identify a novel Z-line to I-band linking system. *Circ Res*. 2001;89(11):1065-1072. doi:10.1161/hh2301.100981
15. Bagnato P, Barone V, Giacomello E, Rossi D, Sorrentino V. Binding of an ankyrin-1 isoform to obscurin suggests a molecular link between the sarcoplasmic reticulum and myofibrils in striated muscles. *J Cell Biol*. 2003;160(2):245-253. doi:10.1083/jcb.200208109
16. Armani A, Galli S, Giacomello E, et al. Molecular interactions with obscurin are involved in the localization of muscle-specific small ankyrin1 isoforms to subcompartments of the sarcoplasmic reticulum. *Exp Cell Res*. 2006;312(18):3546-3558. doi:10.1016/j.yexcr.2006.07.027
17. Lange S, Ouyang K, Meyer G, et al. Obscurin determines the architecture of the longitudinal sarcoplasmic reticulum. *J Cell Sci*. 2009;122(15):2640-2650. doi:10.1242/jcs.046193
18. Pernigo S, Fukuzawa A, Pandini A, et al. The crystal structure of the human titin:obscurin complex reveals a conserved yet specific muscle M-band zipper module. *J Mol Biol*. 2015;427(4):718-736. doi:10.1016/j.jmb.2014.11.019
19. Randazzo D, Giacomello E, Lorenzini S, et al. Obscurin is required for ankyrinB-dependent dystrophin localization and sarcolemma integrity. *J Cell Biol*. 2013;200(4):523-536. doi:10.1083/jcb.201205118
20. Ervasti JM. Costameres: The Achilles' heel of Herculean muscle. *J Biol Chem*. 2003;278(16):13591-13594. doi:10.1074/jbc.R200021200
21. Feher J. Contractile Mechanisms in Skeletal Muscle. *Quant Hum Physiol*. 2017:305-317. doi:10.1016/b978-0-12-800883-6.00028-8
22. Rossi D, Barone V, Giacomello E, Cusimano V, Sorrentino V. The sarcoplasmic reticulum: An organized patchwork of specialized domains. *Traffic*. 2008;9(7):1044-1049. doi:10.1111/j.1600-0854.2008.00717.x
23. Franzini-Armstrong C. The membrane systems of muscle cells. In: *Myology*. ; 2004:232-256.
24. Al-Qusairi L, Laporte J. T-tubule biogenesis and triad formation in skeletal muscle and implication in human diseases. *Skelet Muscle*. 2011;1(1):26. doi:10.1186/2044-

5040-1-26

25. Lu X, Xu L, Meissner G. Activation of the skeletal muscle calcium release channel by a cytoplasmic loop of the dihydropyridine receptor. *J Biol Chem*. 1994;269(9):6511-6516.
26. Dickson EJ. Endoplasmic Reticulum-Plasma Membrane Contacts Regulate Cellular Excitability. *Springer Nat*. 2017. doi:10.1007/978-981-10-4567-7
27. Rosati P, Colombo R, Maraldi N. *Istologia*. V. (Edi Ermes, ed.).
28. Baker JS, McCormick MC, Robergs RA. Interaction among skeletal muscle metabolic energy systems during intense exercise. *J Nutr Metab*. 2010;2010(Figure 1). doi:10.1155/2010/905612
29. Periasamy M, Maurya SK, Sahoo SK, Singh S, Reis FCG, Bal NC. Role of SERCA pump in muscle thermogenesis and metabolism. *Compr Physiol*. 2017;7(3):879-890. doi:10.1002/cphy.c160030
30. Wright EM. Renal Na+-glucose cotransporters ERNEST. *Am J Ren Physiol*. 2001;1751:1-1. doi:10.1109/islc.2004.1382723
31. Abdul-Ghani MA, Norton L, DeFronzo RA. Role of sodium-glucose cotransporter 2 (SGLT 2) inhibitors in the treatment of type 2 diabetes. *Endocr Rev*. 2011;32(4):515-531. doi:10.1210/er.2010-0029
32. Bouché C, Serdy S, Kahn CR, Goldfine AB. The cellular fate of glucose and its relevance in type 2 diabetes. *Endocr Rev*. 2004;25(5):807-830. doi:10.1210/er.2003-0026
33. Zhao F-Q, Keating A. Functional Properties and Genomics of Glucose Transporters. *Curr Genomics*. 2007;8(2):113-128. doi:10.2174/138920207780368187
34. Thorens B, Mueckler M. Glucose transporters in the 21st Century. *Am J Physiol - Endocrinol Metab*. 2010;298(2):141-145. doi:10.1152/ajpendo.00712.2009
35. Tomoichiro A, Katagiri H, Kuniaki T, et al. The Role of N-Glycosylation of GLUT1 for Glucose Transport Activity. *J Biol Chem*. 1991;7266(December 25).
36. Barron CC, Bilan PJ, Tsakiridis T, Tsiani E. Facilitative glucose transporters: Implications for cancer detection, prognosis and treatment. *Metabolism*. 2016;65(2):124-139. doi:10.1016/j.metabol.2015.10.007
37. Alvim RO, Cheuhen MR, Machado SR, Sousa AGP, Santos PCJL. General aspects of muscle glucose uptake. *An Acad Bras Cienc*. 2015;87(1):351-368.

doi:10.1590/0001-3765201520140225

38. Tunduguru R, Thurmond DC. Promoting glucose transporter-4 vesicle trafficking along cytoskeletal tracks: PAK-ing them out. *Front Endocrinol (Lausanne)*. 2017;8(NOV):1-15. doi:10.3389/fendo.2017.00329

39. Shepherd PR, Kahn BB. Glucose transporters and insulin action; implications for Insulin Resistance and Diabetes Mellitus. *N Engl J Med*. 1999:248-257.

40. Mîinea CP, Sano H, Kane S, et al. AS160, the Akt substrate regulating GLUT4 translocation, has a functional Rab GTPase-activating protein domain. *Biochem J*. 2005;391(1):87-93. doi:10.1042/BJ20050887

41. Thorn SL, Gollob MH, Harper ME, Beanlands RS, Dekemp RA, Dasilva JN. Chronic AMPK activity dysregulation produces myocardial insulin resistance in the human Arg302Gln-PRKAG2 glycogen storage disease mouse model. *EJNMMI Res*. 2013;3(1):1-9. doi:10.1186/2191-219X-3-48

42. Jessen N, Goodyear LJ. Invited review: Contraction signaling to glucose transport in skeletal muscle. *J Appl Physiol*. 2005;99(1):330-337. doi:10.1152/japplphysiol.00175.2005

43. Cartee GD. Roles of TBC1D1 and TBC1D4 in insulin- and exercise-stimulated glucose transport of skeletal muscle. *Diabetologia*. 2015;58(1):19-30. doi:10.1007/s00125-014-3395-5

44. Motoshima H, Araki E, Nishiyama T, et al. Bradykinin enhances insulin receptor tyrosine kinase in 32D cells reconstituted with bradykinin and insulin signaling pathways. *Diabetes Res Clin Pract*. 2000;48(3):155-170. doi:10.1016/S0168-8227(00)00121-2

45. Merry TL, Lynch GS, McConell GK. Downstream mechanisms of nitric oxide-mediated skeletal muscle glucose uptake during contraction. *Am J Physiol - Regul Integr Comp Physiol*. 2010;299(6):1656-1665. doi:10.1152/ajpregu.00433.2010

46. Löffler MG, Birkenfeld AL, Philbrick KM, et al. Enhanced fasting glucose turnover in mice with disrupted action of TUG protein in skeletal muscle. *J Biol Chem*. 2013;288(28):20135-20150. doi:10.1074/jbc.M113.458075

47. L. R, S. M. Y, E. O, Thurmond DC. Munc18c: A Controversial Regulator of Peripheral Insulin Action. *Trends Endocrinol Metab*. 2014;(1):21. doi:10.1038/jid.2014.371

48. Antonescu CN, Foti M, Sauvonnet N, Klip A. Ready, set, internalize: Mechanisms

and regulation of GLUT4 endocytosis. *Biosci Rep*. 2009;29(1):1-11. doi:10.1042/BSR20080105

49. Foley K, Boguslavsky S, Klip A. Endocytosis, recycling, and regulated exocytosis of glucose transporter 4. *Biochemistry*. 2011;50(15):3048-3061. doi:10.1021/bi2000356

50. Defronzo RA, Jacot E, Jequier E, Maeder E, Wahren J, Felber JP. The Effect of Insulin on the Disposal of Intravenous Glucose. *Diabetes*. 1981;590(14):1000-1007. doi:10.1113/jphysiol.2012.235127

51. Egan B, Zierath JR. Exercise metabolism and the molecular regulation of skeletal muscle adaptation. *Cell Metab*. 2013;17(2):162-184. doi:10.1016/j.cmet.2012.12.012

52. Stump CS, Henriksen EJ, Wei Y, Sowers JR. The metabolic syndrome: Role of skeletal muscle metabolism. *Ann Med*. 2006;38(6):389-402. doi:10.1080/07853890600888413

53. Ali O. Genetics of type 2 diabetes. *World J Diabetes*. 2013;31(4):114-123. doi:10.1159/000439418

54. Scott LJ, Erdos MR, Huyghe JR, et al. The genetic regulatory signature of type 2 diabetes in human skeletal muscle. *Nat Commun*. 2016;7. doi:10.1038/ncomms11764

55. Sun W, Yao S, Tang J, et al. Integrative analysis of super enhancer SNPs for type 2 diabetes. *PLoS One*. 2018;13(1):1-16. doi:10.1371/journal.pone.0192105

56. Soranzo N, Sanna S, Wheeler E, et al. Common variants at ten genomic loci influence hemoglobin A. *Diabetes*. 2010;59(December):1-27. doi:10.2337/db10-0502.N.S.

57. Imamura M, Maeda S, Yamauchi T, et al. A single-nucleotide polymorphism in ANK1 is associated with susceptibility to type 2 diabetes in Japanese populations. *Hum Mol Genet*. 2012;21(13):3042-3049. doi:10.1093/hmg/dds113

58. Harder MN, Ribel-Madsen R, Justesen JM, et al. Type 2 diabetes risk alleles near BCAR1 and in ANK1 associate with decreased β-cell function whereas risk alleles near ANKRD55 and GRB14 associate with decreased insulin sensitivity in the danish Inter99 cohort. *J Clin Endocrinol Metab*. 2013;98(4):801-806. doi:10.1210/jc.2012-4169

59. Zhou D, Williams MW, Bloch RJ, Birkenmeier CS, Sharp JJ, Barker JE. Small,

membrane-bound, alternatively spliced forms of ankyrin 1 associated with the sarcoplasmic reticulum of mammalian skeletal muscle. *J Cell Biol*. 1997;136(3):621-631. doi:10.1083/jcb.136.3.621

60. Birkenmeier CS, Sharp JJ, Gifford EJ, Deveau SA, Barker JE. An alternative first exon in the distal end of the erythroid ankyrin gene leads to production of a small isoform containing an NH2-terminal membrane anchor. *Genomics*. 1998;50(1):79-88. doi:10.1006/geno.1998.5305

61. Gallagher PG, Forget BG. An alternate promoter directs expression of a truncated, muscle-specific isoform of the human ankyrin 1 gene. *J Biol Chem*. 1998;273(3):1339-1348. doi:10.1074/jbc.273.3.1339

62. Yan R, Lai S, Yang Y, et al. A novel type 2 diabetes risk allele increases the promoter activity of the muscle-specific small ankyrin 1 gene. *Sci Rep*. 2016;6:1-11. doi:10.1038/srep25105

63. Bennett V. Purification of an active proteolytic fragment of the membrane attachment site for human erythrocyte spectrin. *J Biol Chem*. 1978;253(7):2292-2299.

64. Davis JQ, Bennett V. Brain ankyrin. A membrane-associated protein with binding sites for spectrin, tubulin, and the cytoplasmic domain of the erythrocyte anion channel. *J Biol Chem*. 1984;259(21):13550-13559.

65. Peters LL et al. Ank3 (epithelial ankyrin), a widely distributed new member of the ankyrin gene family and the major ankyrin in kidney, is expressed in alternatively spliced forms, including forms that lack the repeat domain. *J Cell Biol*. 1995;130(2):313-330. doi:10.1083/jcb.130.2.313

66. Kordeli E, Lambert S, Bennett V. Ankyrin. *J Biol Chem*. 1995;270(5):2352-2359. doi:10.1074/jbc.270.5.2352

67. Bennett V, 1. Bennett V, Chen L. Ankyrins and cellular targeting of diverse membrane proteins to physiological sites. Curr Opin Cell Biol. 2001;13(1):61-67. doi:10.1016/S0955-0674(00)00175-7Chen L. Ankyrins and cellular targeting of diverse membrane proteins to physiological sites. *Curr Opin Cell Biol*. 2001;13(1):61-67. doi:10.1016/S0955-0674(00)00175-7

68. Lux SE. Anatomy of the red cell membrane skeleton: Unanswered questions. *Blood*. 2016;127(2):187-199. doi:10.1182/blood-2014-12-512772

69. Mohler PJ, Bennett V. Defects in ankyrin-based cellular pathways in metazoan

physiology. *Lincolin Arsyad*. 2005;3(2):1-46. doi:http://dx.doi.org/110.21043/equilibrium.v3i2.1268

70. Cunha SR, Mohler PJ. Ankyrin protein networks in membrane formation and stabilization. *J Cell Mol Med*. 2009;13(11-12):4364-4376. doi:10.1111/j.1582-4934.2009.00943.x

71. Bennett V, Baines AJ. Spectrin and Ankyrin-Based Pathways: Metazoan Inventions for Integrating Cells Into Tissues. *Physiol Rev*. 2017;81(3):1353-1392. doi:10.1152/physrev.2001.81.3.1353

72. Hoock TC, Peters LL, Lux SE. Isoforms of ankyrin-3 that lack the NH2-terminal repeats associate with mouse macrophage lysosomes. *J Cell Biol*. 1997;136(5):1059-1070. doi:10.1083/jcb.136.5.1059

73. Devarajan P, Stabach PR, Mann AS, Ardito T, Kashgarian M, Morrow JS. Identification of a small cytoplasmic ankyrin (AnkG19) in the kidney and muscle that binds βI∑* spectrin and associates with the golgi apparatus. *J Cell Biol*. 1996;133(4):819-830. doi:10.1083/jcb.133.4.819

74. Hopitzan AA, Baines AJ, Ludosky MA, Recouvreur M, Kordeli E. Ankyrin-G in skeletal muscle: Tissue-specific alternative splicing contributes to the complexity of the sarcolemmal cytoskeleton. *Exp Cell Res*. 2005;309(1):86-98. doi:10.1016/j.yexcr.2005.04.013

75. Gagelin C, Constantin B, Deprette C, et al. Identification of AnkG107, a muscle-specific ankyrin-G isoform. *J Biol Chem*. 2002;277(15):12978-12987. doi:10.1074/jbc.M111299200

76. Giacomello E, Sorrentino V. Localization of ank1.5 in the sarcoplasmic reticulum precedes that of SERCA and RyR: Relationship with the organization of obscurin in developing sarcomeres. *Histochem Cell Biol*. 2009;131(3):371-382. doi:10.1007/s00418-008-0534-4

77. Giacomello E. Deletion of small ankyrin 1 (sAnk1) isoform results in structural and functional alterations in aging skeletal muscle fibers. *Am J Physiol*. 2015.

78. Kontrogianni-Konstantopoulos A, Catino DH, Strong JC, et al. Obscurin modulates the assembly and organization of sarcomeres and the sarcoplasmic reticulum. *FASEB J*. 2006;20(12):2102-2111. doi:10.1096/fj.06-5761com

79. Giacomello E, Quarta M, Paolini C, et al. Deletion of small ankyrin 1 (sAnk1) isoforms results in structural and functional alterations in aging skeletal muscle

fibers. *Am J Physiol Physiol*. 2014;308(2):C123-C138. doi:10.1152/ajpcell.00090.2014

80. Musarò A, McCullagh K, Paul A, et al. Localized Igf-1 transgene expression sustains hypertrophy and regeneration in senescent skeletal muscle. *Nat Genet*. 2001;27(2):195-200. doi:10.1038/84839

81. Pfaffl MW. *A-Z of Quantitative PCR*. (Bustin SA, ed.). La Jolla, CA, USA; 2004. doi:10.1029/JA089iA05p02945

82. Taylor SC, Posch A. The design of a quantitative western blot experiment. *Biomed Res Int*. 2014;2014. doi:10.1155/2014/361590

83. Frasca D, Blomberg BB, Paganelli R. Aging, obesity, and inflammatory age-related diseases. *Front Immunol*. 2017;8(DEC):1-10. doi:10.3389/fimmu.2017.01745

84. Kontrogianni-Konstantopoulos A, Jones EM, van Rossum DB, Block RJ. Fibronectin polymerization regulates the composition and stability of extracellular matrix fibrils and cell-matrix adhesions. *Mol Biol Cell*. 2003;14(February):2372-2384. doi:10.1091/mbc.E02

85. Ackermann MA, Ziman AP, Strong J, et al. Integrity of the network sarcoplasmic reticulum in skeletal muscle requires small ankyrin 1. *J Cell Sci*. 2011;124(21):3619-3630. doi:10.1242/jcs.085159

86. Pierantozzi E, Szentesi P, Al-Gaadi D, et al. Calcium Homeostasis Is Modified in Skeletal Muscle Fibers of Small Ankyrin1 Knockout Mice. *Int J Mol Sci*. 2019;20(13):3361. doi:10.3390/ijms20133361

87. Defronzo RA. Type 2 Diabetes Mellitus. *Nat Rev*. 2016;1(July). doi:10.1016/B978-0-12-803376-0.00012-5

88. Contreras-Ferrat A, Lavandero S, Jaimovich E, Klip A. Calcium signaling in insulin action on striated muscle. *Cell Calcium*. 2014;56(5):390-396. doi:10.1016/j.ceca.2014.08.012

89. Reynolds TH, Dalton A, Calzini L, Tuluca A, Hoyte D, Ives SJ. The impact of age and sex on body composition and glucose sensitivity in C57BL/6J mice. *Physiol Rep*. 2019;7(3):1-9. doi:10.14814/phy2.13995

90. Desmond PF, Muriel J, Markwardt ML, Rizzo MA, Bloch RJ. Identification of small ankyrin 1 as a novel sarco(endo)plasmic reticulum Ca2+-ATPase 1 (SERCA1) regulatory protein in skeletal muscle. *J Biol Chem*. 2015;290(46):27854-27867. doi:10.1074/jbc.M115.676585

91. Sahoo SK, Shaikh SA, Sopariwala DH, Bal NC, Periasamy M. Sarcolipin protein interaction with Sarco(endo)plasmic reticulum CA 2+ ATPase (SERCA) Is distinct from phospholamban protein,and only sarcolipin can promote uncoupling of the serca pump. *J Biol Chem*. 2013;288(10):6881-6889. doi:10.1074/jbc.M112.436915

92. Asahi M, Kurzydlowski K, Tada M, MacLennan DH. Sarcolipin inhibits polymerization of phospholamban to induce superinhibition of sarco(endo)plasmic reticulum Ca2+-ATPases (SERCAs). *J Biol Chem*. 2002;277(30):26725-26728. doi:10.1074/jbc.C200269200